Article

Correction of Terrain Effects on Forest Canopy Height Estimation Using ICESat-2 and High Spatial Resolution Images

Bin Li [1,2,3], Tianzhong Zhao [1,2,3], Xiaohui Su [1,2,3,*], Guangpeng Fan [1,2,3], Wenjie Zhang [1,2,3], Zhuo Deng [1,2,3] and Yonghui Yu [4]

1   School of Information Science and Technology, Beijing Forestry University, Beijing 100083, China
2   Engineering Research Center for Forestry—Oriented Intelligent Information Processing,
     National Forestry and Grassland Administration, Beijing 100083, China
3   Forestry Information Research Institute, Beijing Forestry University, Beijing 100083, China
4   Guangxi Gaofeng Forest Farm, Nanning 530001, China
*   Correspondence: suxhui@bjfu.edu.cn

Abstract: The Ice, Cloud, and Land Elevation Satellite–2 (ICESat–2) carries the Advanced Topographic Laser Altimeter System (ATLAS), enabling global canopy height measurements from forest canopy height models (CHMs). Topographic slope is a crucial factor affecting the accuracy of canopy height estimates from ICESat–2 CHMs, but it has not been sufficiently studied. This paper aims to eliminate the influence of slope on canopy height estimates from ICESat–2 data and establishes a method for correcting forest canopy heights based on high spatial resolution digital orthophoto maps (DOM). The cross-track photons are corrected horizontally to eliminate the estimation error. Multi-resolution segmentation is used to segment tree crowns in the DOM, and the distance and relative position between the top of canopy (TOC) photons and the center point of the crown are calculated. TOC photon correction rules are established for different terrains, and the vertical error of the TOC photons is corrected. The results indicate that the vertical error increases exponentially with the slope. The cross-track photon correction and the TOC photon correction method eliminate the effect of slope on canopy height estimates. The cross-track photon correction method reduces the mean absolute error (MAE) and root mean square error (RMSE) of the canopy height estimates by 35.71% and 35.98%, respectively. The TOC photon correction approach further reduces the MAE and RMSE by 23% and 19.23%, respectively. The proposed method has significantly higher accuracy for forest canopy height estimation using ICESat–2 data than the traditional method.

Keywords: ICESat–2/ATLAS; canopy height model; slope; multi-resolution segmentation; correction

1. Introduction

Vegetation canopy height is a critical input parameter for vegetation biomass modeling, which is crucial for tracking the spatial and temporal dynamics of forest ecosystems [1–3] and providing information on how the carbon cycle and terrestrial ecosystems affect the future climate [4–6]. Airborne laser scanning (ALS) is a relatively mature method widely used in modern forest monitoring and has replaced fieldwork in many cases [7–9]. Although a growing number of countries are acquiring ALS data, collecting these data over large areas is extremely expensive. Current opportunities for obtaining large-scale LiDAR data are provided by the Global Ecosystem Dynamics Investigation (GEDI) project and the Ice, Cloud, and Land Elevation Satellite–2 (ICESat-2) [10–12].

The Advanced Topographic Laser Altimeter System (ATLAS) onboard ICESat–2 is a single-photon sensitive LiDAR system capable of detecting individual photons from reflected pulses [13–15]. ICESat–2 has 4 levels of 22 products, ATL00~ATL21. ATL03 and ATL08 are digital elevation model (DTM) and digital surface model (DSM) products. ATL03 is the global geolocated photon data, and ATL08 is the land and vegetation height data. The latter is a collection of ground and canopy elevations obtained by filtering the

ATL03 point cloud with the differential, regressive, and Gaussian adaptive nearest neighbor algorithm. Inversion is performed using a surface finding algorithm, which identifies the ground elevation and relative canopy height every 100 m along the track [6,16]. ICESat–2 spaceborne LiDAR is based on state-of-the-art technology, but its accuracy for forest height measurements remains to be verified [17,18].

Unlike airborne LiDAR systems, spaceborne LiDAR systems such as ICESat–2 have the advantage of large-area coverage. However, the fundamental question is whether they can replace airborne LiDAR for forest height measurements to reduce costs. Gwenzi et al. [19] used Multiple Altimeter Beam Experimental Lidar (MABEL) data and simulated ATLAS data for canopy height estimation in savanna ecosystems. It was concluded that the number of signal photons in the ATLAS data was significantly lower than that of the airborne experimental data (MABEL), resulting in lower accuracy of canopy height estimation. Popescu et al. [20] used the MABEL data and obtained average RMSE values of 2.70 m and 3.59 m for nighttime and daytime canopy height estimations, respectively. Narine et al. [21] used simulated ICESat–2 photon-counting LiDAR data to analyze the relationship between photon-counting vegetation products and canopy cover obtained in noiseless scenes, daytime scenes, and nighttime scenes. Several inversion studies using simulated ICESat–2 data showed a correlation between forest structure parameters in the MABEL inversion and those in the airborne point cloud data inversion. However, there are still significant differences in the noise distribution, operating environment, and surface vegetation height estimates between the MABEL and ICESat–2 photon cloud data. Malambo [6], Neuenschwander [22], and Liu [23] evaluated the agreement between canopy height estimates obtained from the ATL08 product of ICESat–2 and airborne LiDAR data in the United States and Finland. Their results indicated high accuracy of ATL08 in areas with moderate vegetation cover. In forest-covered areas, an ICESat–2 spot returned only a few signal photons, whose vertical positions were uncertain in the canopy [24,25]. Since the top of canopy (TOC) photons are not necessarily located at the top of the canopy, forest canopy height estimates obtained from ATLAS data are often lower than the true height [22]. A comparison of airborne LiDAR data and ICESat–2 data showed that photon-counting LiDAR could reflect the vertical structure of the forest.

Most studies on canopy height estimates based on ICESat–2 data have first used a point cloud filtering algorithm [26–28]. Subsequently, canopy height extraction is achieved by subtracting the terrain surface elevation from the top photon elevation of the canopy [29]. Few scholars have considered the influence of terrain on canopy height extraction. It has been reported that the error in canopy height estimates obtained from ICESat–2 increases with the increasing slope [17,30]. The extraction of canopy heights from ATL08 is influenced by complex surface factors such as the topographic slope [23]. Extracting terrain and canopy heights from ATL08 is particularly challenging on steep slopes (>30°) [6]. Most studies did not consider slope a critical parameter for canopy height extraction from ICESat–2 data. Various factors contribute to errors in LiDAR-based canopy height estimations, such as topography, forest type, forest structure, and point cloud filtering algorithms, and the terrain plays a key role [31,32]. These studies have shown that terrain relief can increase or decrease the distance between the highest point of the canopy and the lowest point of the ground, resulting in errors. Hence, it is necessary to incorporate single-photon detection to correct the heights of the TOC photons.

ICESat–2 data are increasingly used by the scientific community, but few studies have validated its canopy height estimates. Spaceborne LiDAR differs from airborne and ground-based LiDAR in that its sensors are a long distance from the ground, and the photon positions are susceptible to distortions due to terrain, especially in mountainous areas with large terrain relief. A study on canopy height detection using ICESat–2 data reported that slope was the most influential factor affecting the accuracy of canopy height estimation [33]. Wang et al. [34] and Zhang et al. [35] proposed a vegetation-based semi-analytic echo model to reduce canopy height estimation errors. Wang et al. [25] analyzed the effects of the foliage area, density, and canopy shape on ICESat–2 canopy height estimations. However,

the authors did not report the source of the slope error and whether it could be eliminated. Determining the errors in forest height estimates due to slope in complex topographic areas has become a critical issue for using ICESat–2 data for large-scale biomass estimation. A methodology to attenuate the influence of surface terrain on canopy height estimates is urgently needed.

The objective of this study is to propose a physical geometric correction model based on high spatial resolution digital orthophoto map (DOM) data to correct canopy height estimates and improve the accuracy of ICESat–2 canopy parameter extraction in complex terrain. We focus on the following aspects: (1) we establish an ICESat–2 canopy height correction method that eliminates the effect of slope to enable ICESat–2 canopy height inversion. (2) We investigate the accuracy of ATL03 and ATL08 canopy data in subtropical regions and the effect of different window sizes and percentages of canopy height parameters on forest canopy height estimation. (3) The effects of the photon offset distance, canopy relief rate, and canopy density on the inversion accuracy of the canopy height estimates derived from the point cloud are analyzed. The results of this study provide new methods and ideas for ICESat–2 canopy data extraction in complex terrain.

2. Materials and Methods

2.1. Study Area

The study area is a forested region in Nanning City, Guangxi Zhuang Autonomous Region, China (22.57°N~23.00°N, 108.23°E~108.24°E (cf. Figure 1). Nanning City has a subtropical monsoon climate, with an annual average temperature of about 21.6 °C and average annual precipitation of 1241~1753 mm [36]. The study area is hilly land with an elevation range of 120~360 m (World Geodetic System 1984, WGS84) and a slope range of 0°~51°, with slope greater than 15° accounting for 64.46% of the study area. The study area has coniferous, broadleaf, and mixed coniferous forests. The forest cover exceeds 92%, and the canopy height has a range of 0.1~24.6 m. The average tree density is 1300 trees per hectare, the average stand basal area is 11.30 m^2/hm^2, and the average stand volume is 147.47 m^3.
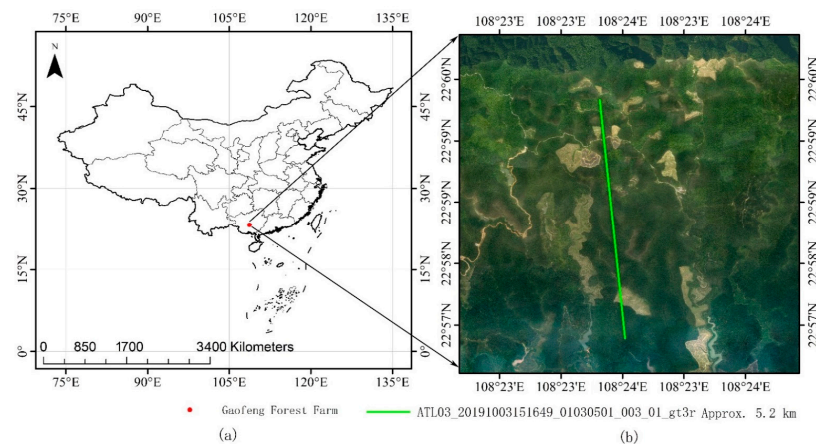
Figure 1. Location of study area: (**a**) location of the forest farm site in China; (**b**) a subset of the footprint of the ICESat–2 data with 5.2 km (where 5.2 km is the distance of that along-track).

2.2. Research Data

2.2.1. ICESat–2 Data

ICESat–2 has an average orbital altitude of 496 km (±6 km) and covers an area ranging from 88°N to 88°S [30,37,38]. The footprint of ATLAS has a diameter of about 14 m and a footprint spacing of 0.7 m along the track [39]. ATLAS uses three pairs of beams, each pair consisting of a laser beam with intensity-to-weak beam energy ratio of 4:1 [12] (cf. Figure 2). During the light pulse emission, the photon triggers a timer as it passes through the beam splitter and when it returns and passes through the filter. The time-

stamped data of the returning photons are transmitted to the ground via the electronics and communication system on ICESat–2. The WGS84 ellipsoidal heights of the surface are determined by calculating the position of the spacecraft and the distance traveled by the photon (https://icesat--2.gsfc.nasa.gov/space-lasers, accessed on 20 October 2021). This study only analyzed the canopy height of strong nighttime beams. The track ID numbers are ATL03_20191003151649_01030501_003_01_gt3r and ATL08_2019100 3151649_01030501 _003_01_gt3r, and the data were obtained on 3 October 2019 from https://search.earthdata.nasa.gov (accessed on 5 March 2021).
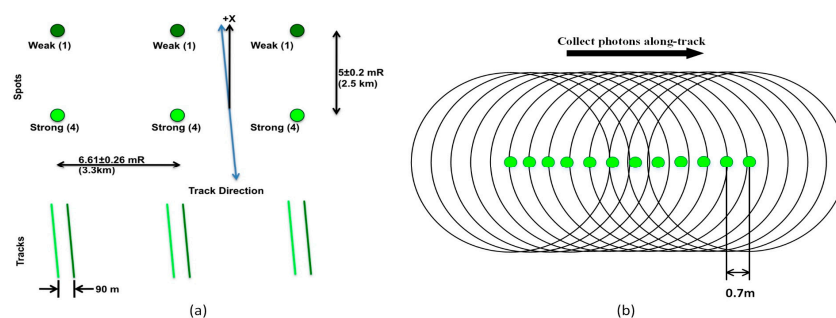
Figure 2. ICESat–2/ATLAS data acquisition mode: (**a**) laser beam distribution (https://icesat--2.gsfc.nasa.gov/science/specs, accessed on 20 October 2021); and (**b**) schematic diagram of sampling spacing interval.

2.2.2. ALOS PALSAR DEM Data

The Advanced Land Observing Satellite (ALOS) has a Phased Array type L-band Synthetic Aperture Radar (PALSAR) capable of almost all-weather observations [40]. The ALOS PALSAR DEM has a pixel size of 12.5 m [41]. The file (AP\U 16054\U FBS\U F0440\U RT1) was downloaded from https://asf.alaska.edu (accessed on 20 March 2021) and contained data obtained in October 2018. Due to the relatively high pixel resolution and accuracy of ALOS PALSAR DEM data, it is used as the reference elevation data.

2.2.3. CAF–LiCHy LiDAR Data

A LiDAR sensor with a small spot size is preferable for evaluating the spatial structure of forests [42–44]. The Institute of Resource Information at the Chinese Academy of Forestry has developed an integrated remote sensing observation platform called CAF–LiCHy (Chinese Academy of Forestry, LiDAR, CCD, Hyperspectral). The system consists of a full-waveform airborne lidar (Riegl LMS–Q680i) system, an airborne push-broom hyperspectral scanner (AISA Eagle II), and a high-resolution charge-coupled device (CCD) camera (DigiCAM–H60) [15,45]. The CAF–LiCHy is similar to the LiDAR Hyperspectral Thermal (G–LiHT) system of the National Aeronautics and Space Administration (NASA) Goddard Space Flight Center. The CHM extracted from the CAF–LiCHy LiDAR data was used to verify the accuracy of the canopy height model (CHM) obtained from the ATLAS data. The spatial resolution and vertical accuracy of the CAF–LiCHy data are 1.0 m and 0.15 m, respectively (cf. Table 1). We obtained data in April 2018 in the WGS—84 coordinate system.

Table 1. The parameters of the sensors of the CAF–LiCHy system [45].

LiDAR: Riegl LMS–Q680i			
Wavelength	1550 nm	Laser beam divergence	0.5 mrad
Laser pulse length	3 ns	Cross-track FOV	±30°
Maximum laser pulse repetition rate	400 khz	Waveform sampling interval	1 ns
Vertical resolution	0.15 m	Point density @1000 m altitude	3.6 pts/m^2
CCD: DigiCAM–60			
Frame size	8956 × 6708	Pixel size	6 μm
Imaging sensor size	40.30 mm × 53.78 mm	Focal length	50 mm
FOV	56.2°	Spatial resolution	0.2 m

2.2.4. Ancillary Image Data

Ancillary image data included DOM data from the CAF–LiCHy system and high-resolution satellite image data from Google Earth. The DOM data were acquired by the CCD digital camera (DigiCAM–H60), which has a focal length of 50 mm. The images have 60 million pixels and 0.2 m spatial resolution [45]. The data were obtained in April 2018. Table 1 list the sensors' parameters. The satellite image data from Google Earth were L19 level (spatial resolution of approx. 0.3 m) and were acquired in March 2018 and accessed on 7 August 2022. The image data had a GeoTIFF file format and were in the WGS-84 vertical coordinate system.

2.3. Methodologies

The estimation of canopy height parameters requires explicit TOC and ground photon signals. In this study, the ICESat–2 data processing included cross-track photon correction, photon denoising, photon classification, TOC photon correction, canopy parameter extraction, and accuracy evaluation. The canopy heights obtained from the ATL08 data (CHM $_{ATL08}$), ATL03 original data (CHM $_{ATL03\ initial}$), ATL03 data after cross-track photon correction (CHM $_{CTPC}$), ATL03 data after cross-track photon correction and Google Image data after canopy height correction (CHM $_{CCR–1}$), and ATL03 data after cross-track photon correction and airborne image canopy height correction (CHM $_{CCR–2}$) were compared with the CHM$_{ALS}$ extracted from the CAF-LiCHy LiDAR Data. Figure 3 depicts the flowchart of the inversion of different CHMs.
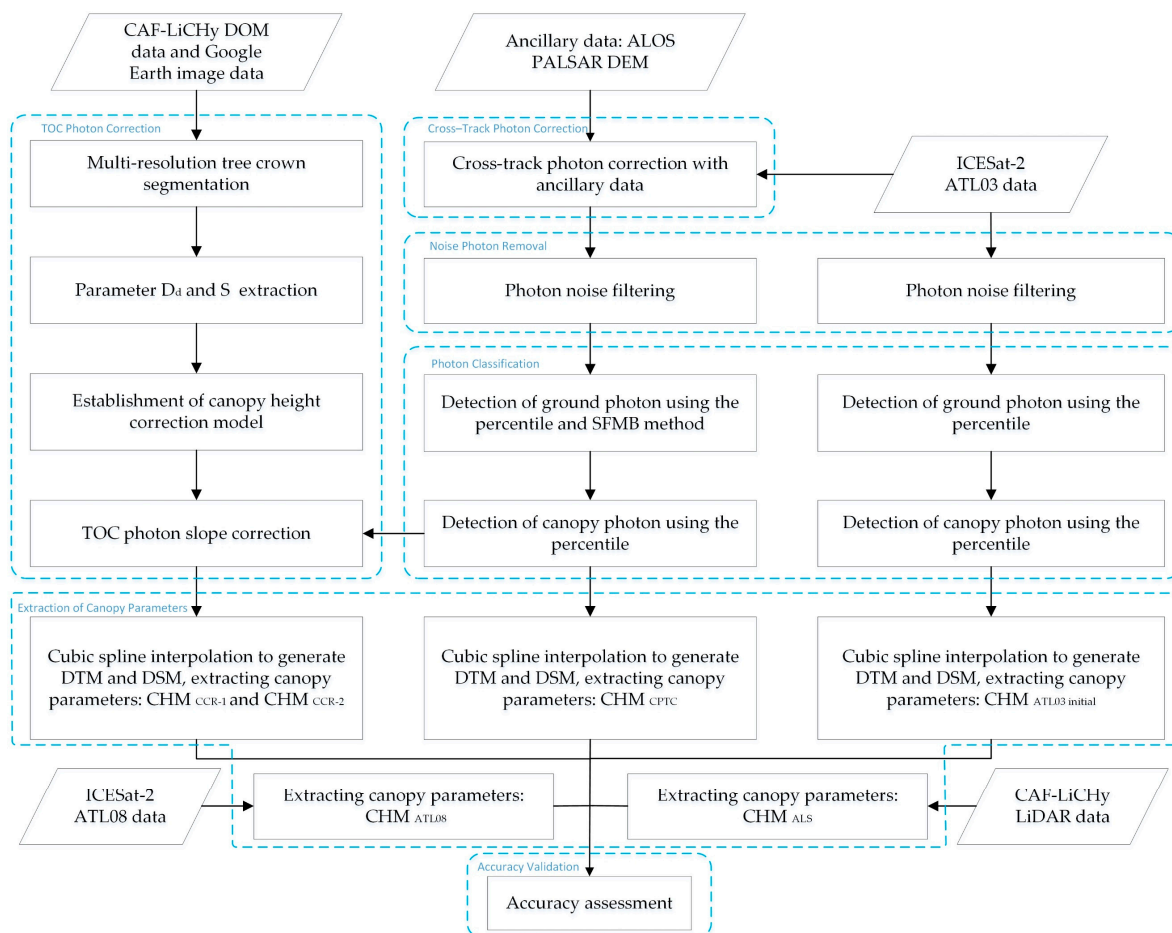
Figure 3. Methodology flowchart.

2.3.1. Cross-Track Photon Correction

A 6.5 m cross-track horizontal offset of the photons is allowed [40,46], and the distance of the photon's cross-track on flat land or on low slopes does not affect the ground elevation and canopy height estimation. However, on large slopes and complex terrain, disregarding the cross-track offset of the photons might cause errors in the DTM and DSM (cf. Figure 4a). Figure 4d shows an irregular distribution of photons on each side of the track, indicating that the cross-track offsets are not the same. Therefore, before the photon data were transformed into a photon point cloud, photon correction was performed using the cross-track photon correction method proposed by Li et al. [47]. First, we obtained the mapping points of the cross-track photons (Equation (1)). The reference elevations of the original photon (P) and the mapping point (P') of ATL03 were extracted from the ALOS PALSAR DEM (a cubic interpolation method was used to interpolate the DEM to 1.0 m spatial resolution) as the reference elevations z_0 and z_1 of the original photon and the mapping point, respectively. Photons with a cross-track distance ≥ 0.50 m or ≤ -0.50 m were corrected to the reference ground track (cf. Figure 4c), and the corrected photon elevation was obtained from Equation (2).

$$\begin{bmatrix} x_0 \\ y_0 \end{bmatrix} = f\left(\begin{bmatrix} x_1 \\ y_1 \end{bmatrix} \right) \tag{1}$$

$$E_c = E_i - (z_0 - z_1) \tag{2}$$

where x_0, y_0 are the original latitude and longitude of the ATL03 photon, respectively; x_1, y_1 are the latitude and longitude of the mapping point, respectively; z_0, z_1 are the original elevations of the photon and mapping point, respectively, E_C is the elevation of the mapping point, and E_i is the original elevation of the ATL03 photon.
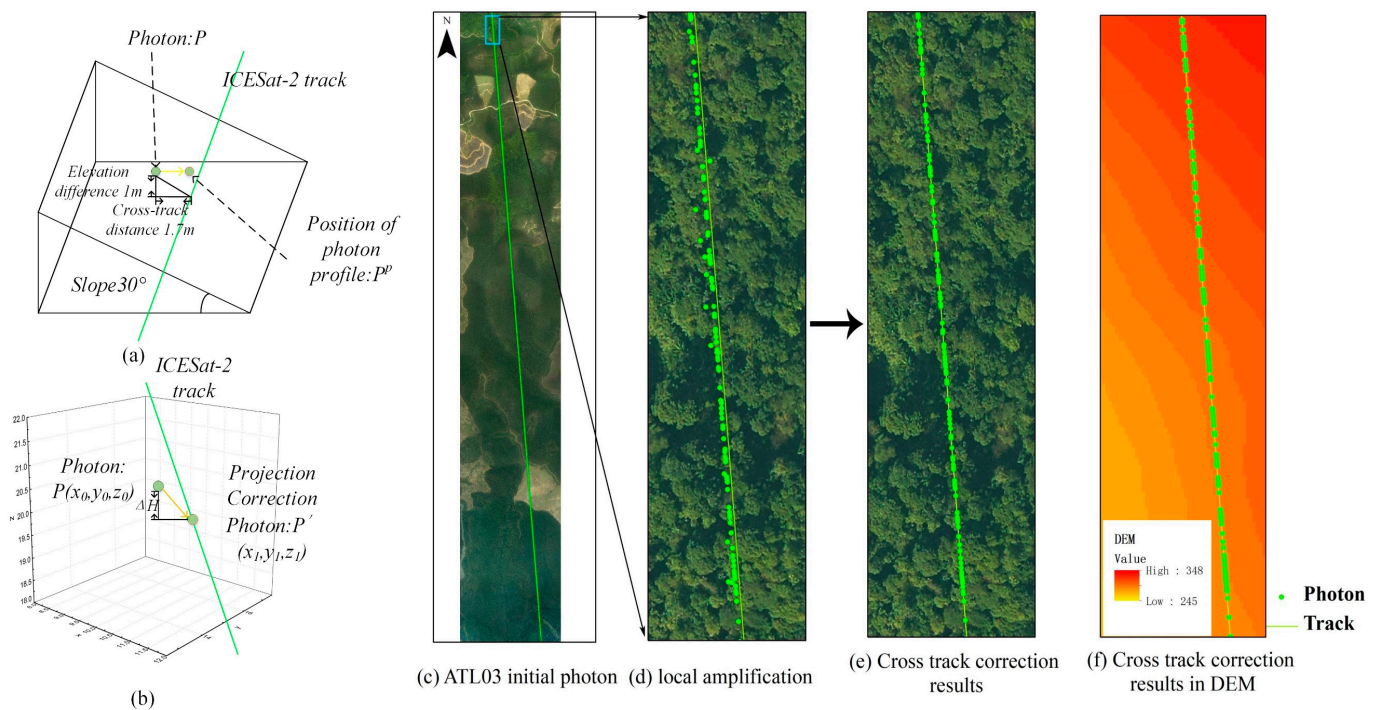
Figure 4. Schematic of the photon position before and after correction: (**a**) schematic of the cross-track photon error [47]; (**b**) schematic of correcting the cross-track photon error [47]; (**c,d**) positions of the initial photons; (**e**) photons after correction of (**d,f**) cross-track correction results for the ALOS PALSAR DEM.

2.3.2. Noise Photon Removal

The photon's geographic location was converted to the along-track distance (ATD) before noise removal. The data were first coarsely denoised to narrow down the range of possible signal photons. The photon cloud data were divided into different along-track photon cloud data using a window size of 20 m in the ATD. Histograms of the elevation statistics were calculated, and the histogram peak positions were obtained for each window. They were used as the center position of the signal photons, and an elevation threshold was set near the center position to establish a buffer of photon signals (Equations (3) and (4)). Subsequently, we removed the noise photons outside the buffer.

$$minr = h_\alpha - 3\sigma \tag{3}$$

$$maxr = h_\alpha + 3\sigma \tag{4}$$

where minr is the minimum elevation, maxr is the maximum elevation, h_α is the elevation at the histogram peak position, and σ is the standard deviation of the photon elevation within each window.

The improved Ordering Points to Identify the Clustering Structure (OPTICS) algorithm proposed by Zhu et al. [17] was used for fine denoising. The improved OPTICS algorithm consists of three steps. First, an elliptical search region was established. Second, the core distance and reachable distance of each photon were calculated based on the neighborhood radius and neighborhood minimum number of points. Third, the photons were sorted according to the reachable distance from smallest to largest, and the optimal reachable distance threshold of each window was determined using the maximum inter-class variance algorithm. Photons larger than the threshold were regarded as noise points, and the others were regarded as signal points. Figure 5a shows the ATL03 cross-track correction data and the result after noise removal.

2.3.3. Photon Classification

Following photon noise removal, the data contained few ground photons and numerous TOC photons, making it difficult to distinguish them and accurately depict the terrain and canopy [48]. An overlapping moving window was created to identify the ground and canopy photons.

We provide a brief summary of the methods used to classify ground photons. They include overlapping moving windows, the percentile method, and the slope filtering method. First, a window was created. A correlation exists between the extraction error and the extraction window size and step size [40,41,49]. Preliminary investigations indicated that the moving window width to detect ground photons should be 20 m, and the moving step length should be 10 m to enable the precise extraction of the photons of interest. Second, an elevation percentile range was selected to extract potential ground photons within the window range. Since the ATL03 data in this region had a low photon density, photons in the elevation percentile range of [0.00, 0.15] were chosen to ensure that a sufficient number of photons were available for terrain height estimation. However, near-ground noise photons and near-ground vegetation photons remained in the photon point cloud after denoising, and the photons in the window elevation percentile range of [0.00, 0.15] were not necessarily all ground photons. Ground photons have a continuous distribution, whereas near-ground noise photons and near-ground vegetation photons lack continuity compared with the elevation values of neighboring points. These photons are prone to sudden elevation changes (sudden increase or decrease) because the data have not been smoothed. The slope filtering method (SFMB) proposed by Li et al. [47] was used to minimize the effect of near-ground photon noise on ground photon extraction and extract possible ground photons obtained in the previous step. The SFMB method consists of two steps.
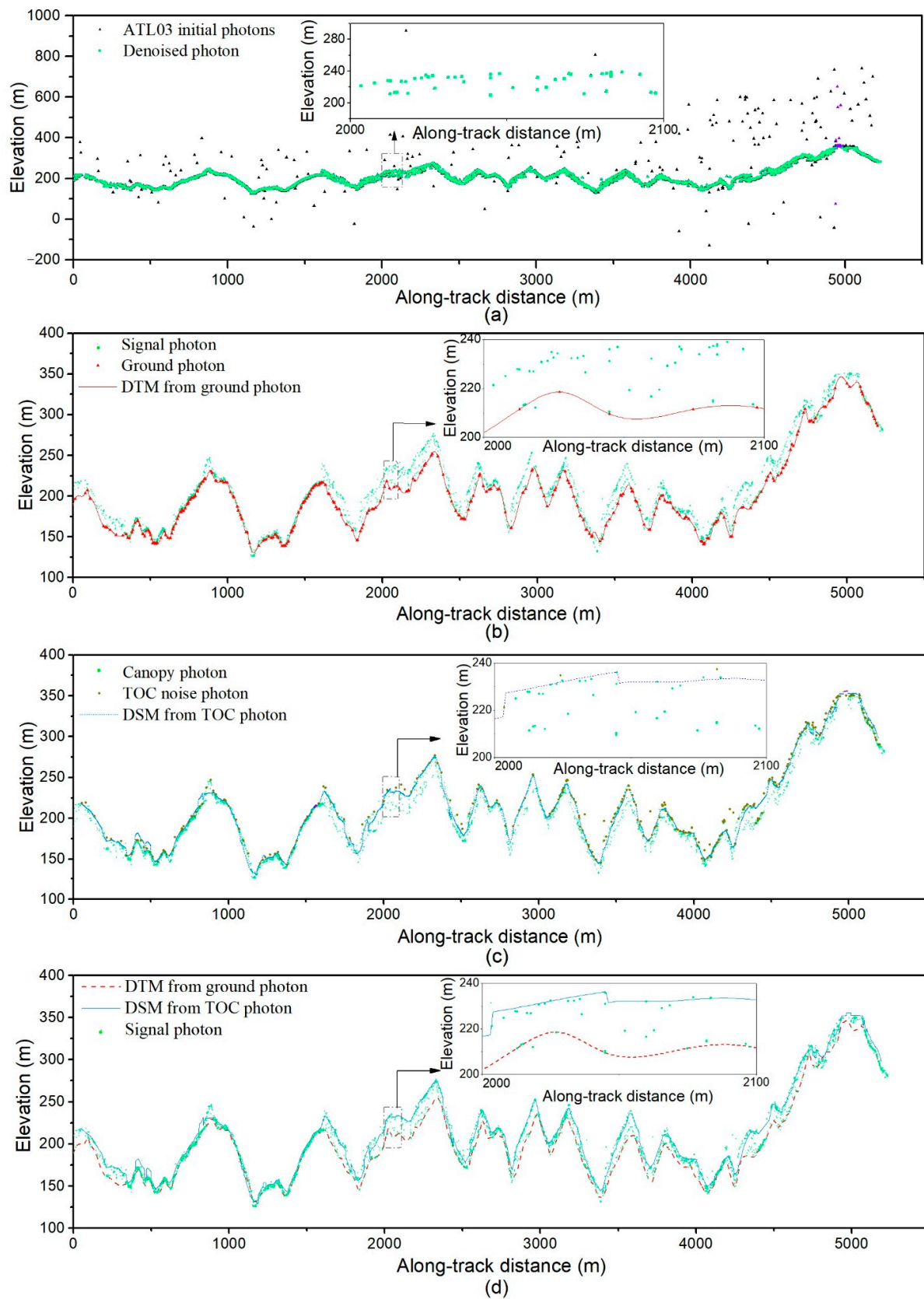
Figure 5. Photon denoising and classification results: (**a**) result of photon denoising; (**b**) result of ground photon extraction and ground surface fitting; (**c**) photon extraction and surface fitting of vegetation canopy; (**d**) DTM and DSM generated by cubic spline interpolation.

The slope of the possible ground photons was calculated, and the maximum slope in the reference elevation data ALOS PALSAR DEM was used as the threshold value. Photons larger than the threshold value were marked as noise photons. The maximum value of the slope change in the reference elevation data was used as the threshold value, and photons smaller than the threshold value were marked as ground photons. Figure 5b depicts the results (red dots).

The correct extraction of TOC photons may be hampered by photon noise in the photon cloud remaining after denoising [50]. We used the TOC classification method proposed by Popescu et al. [20] to determine the TOC photons. The width of the moving window and the movement steps were the same as for the ground photon classification. The TOC noise photons were those in the given elevation percentile range [0.99, 1] for each moving window. After removing the photons in this percentile range, the elevation percentile was recalculated, and the photon cloud corresponding to the photon elevation percentile range of [0.96, 0.99] was extracted and used as TOC photons. The canopy photon results are shown as green dots in Figure 5c.

2.3.4. TOC Photon Correction
Effect of Slope

The canopy height photon point cloud contains information on the height difference between the DSM and DTM on the same coordinate plane. Although a photon-counting LIDAR system has the advantages of providing high frequency and high-resolution data, the TOC photons are not necessarily located at the top of the canopy, resulting in errors in the canopy height estimation. The difference between the elevation at the TOC and that on the ground should be the canopy height of trees. However, this height difference differs from the real canopy height on slopes (such as on hills, valleys, steep slopes, or degraded places) [51].

When the difference between canopy photon data and DTM was used to compute canopy height, Figure 6 illustrates the impact of the surface slope on canopy height based on the difference between the canopy height of the photon data and the DTM. The LiDAR variable RH100 is defined as the distance between the apex of the canopy and the ground point. On flat land, RH100 is approximately the vegetation canopy height (cf. Figure 6a). When a tree is located on a slope, the photons hit the same position in the canopy, and the difference between the canopy photons and the DTM is h_a'. This parameter has been used as the canopy height in most studies on canopy height inversion based on ICESat–2 data. However, the actual canopy height is the difference between the height of the TOC photons and the height at the point where the tree roots enter the ground, i.e., h_a in Figure 6b. The difference (or error) between h_a and h_a' is caused by the slope and is defined by Equation (5). The position of the photon relative to the trunk center point affects how the slope error is corrected. Figure 6b,c show this difference at different slope heights. The height discrepancy between causes errors in estimating the canopy height and is largely terrain-induced. Therefore, the effect of topography must be eliminated to extract the canopy height accurately.

The distance between the photon location and the trunk center point (D_d), the relative position, and the slope affect the terrain-induced canopy height error. Table 2 lists the maximum errors for different slopes and different D_d. The vertical displacement caused by the slope increases exponentially with the slope of the terrain. The terrain has a significant impact on canopy height measurements that cannot be ignored in extremely steep terrain. The distance between the TOC photon location and the center point of the crown cannot be directly obtained from probability sampling of ATLAS photons [24,52,53]. Therefore, we utilize crown segmentation to quantify the effect of the distance between the TOC photon location and the center point of the crown on canopy height extraction.

$$h' = h \pm D_d \times \tan(p) \tag{5}$$

where h' is the tree height obtained by inversion, h id actual tree height, D_d is the horizontal distance between the TOC photon location and the center point of the crown, and p is the slope.

•	Photon position	D_d and D_d'	Distance from photon to trunk	h_a', h_b', h_c', h_d' ICESat-2 measuring tree height
H	Actual tree height	p	Angle of the slope gradient	h_a, h_b, h_c, h_d Actual height of ICESat-2 measurement
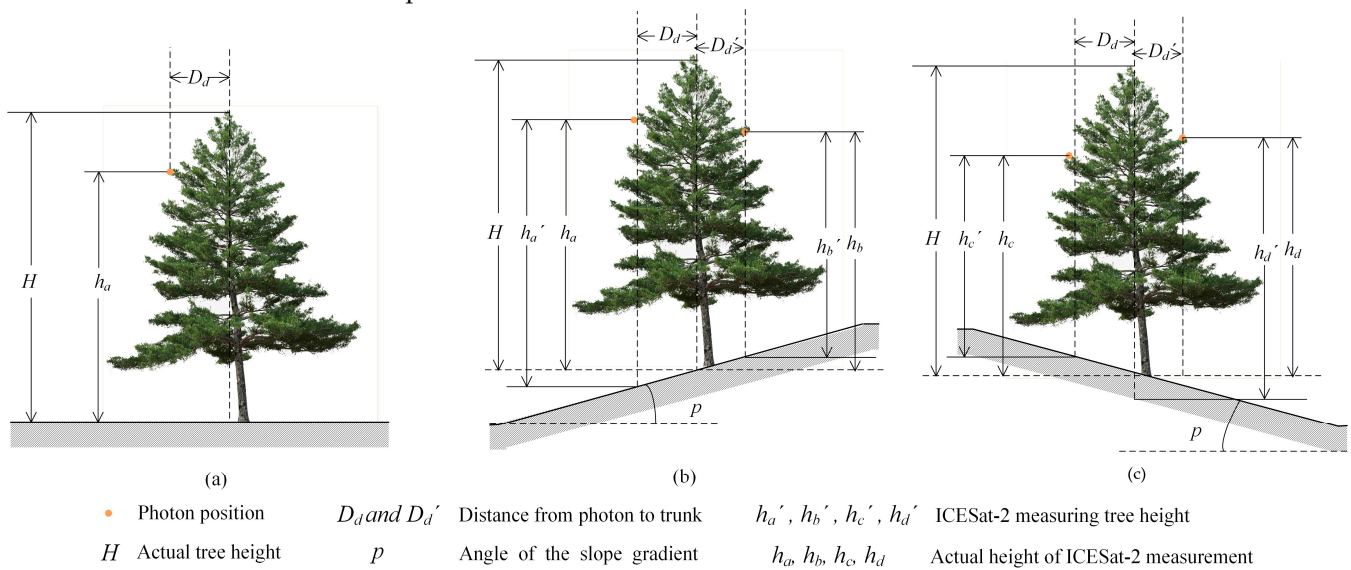
Figure 6. Effect of slope on canopy height estimates at different slope locations: (**a**) canopy height retrieved on flat land; (**b**) canopy height retrieved on a uphill slope; and (**c**) canopy height retrieved on a downhill slope.

Table 2. Maximum error of canopy for different slopes.

Offset Distance/(m)	Slope									
	5°	10°	15°	20°	25°	30°	35°	40°	45°	50°
1	0.09	0.18	0.27	0.36	0.47	0.58	0.70	0.84	1.00	1.19
2	0.17	0.35	0.54	0.73	0.93	1.15	1.40	1.68	2.00	2.38
3	0.26	0.53	0.80	1.09	1.40	1.73	2.10	2.52	3.00	3.58

Crown Segmentation

Multi-resolution segmentation (MS) is commonly used for segmenting ultra-high resolution images [54–56]. We used eCognition software (Definens Developer 8.7) for crown segmentation of the DOM with a resolution of 0.2 m and Google Earth images with a resolution of 0.3 m. A 9 × 9 median filter was applied to the DOM prior to segmentation to prevent over-segmentation [51]. The scale, shape ratio, and compactness ratio are required input parameters for MS in eCognition. The scale parameter affects the average size of the segmented objects, the shape ratio controls the homogeneity, and the compactness ratio influences the object's shape. The optimal segmentation parameters for various forest types were determined after extensive experiments and considering the vegetation structure and distribution. The 0.2 m resolution image had a scale parameter of 12~16, a shape ratio of 0.7~0.8, and a compactness ratio of 0.6~0.9. The 0.3 m resolution image had a scale parameter range of 10~12, a shape ratio range of 0.4~0.5, and a compactness ratio range of 0.6~0.7. The To assure quality, the final segmentation results were visually personally examined for an appropriate segmentation performance. The segmentation results are shown in Figure 7.

(a) —— Crown contour —— Track (b)
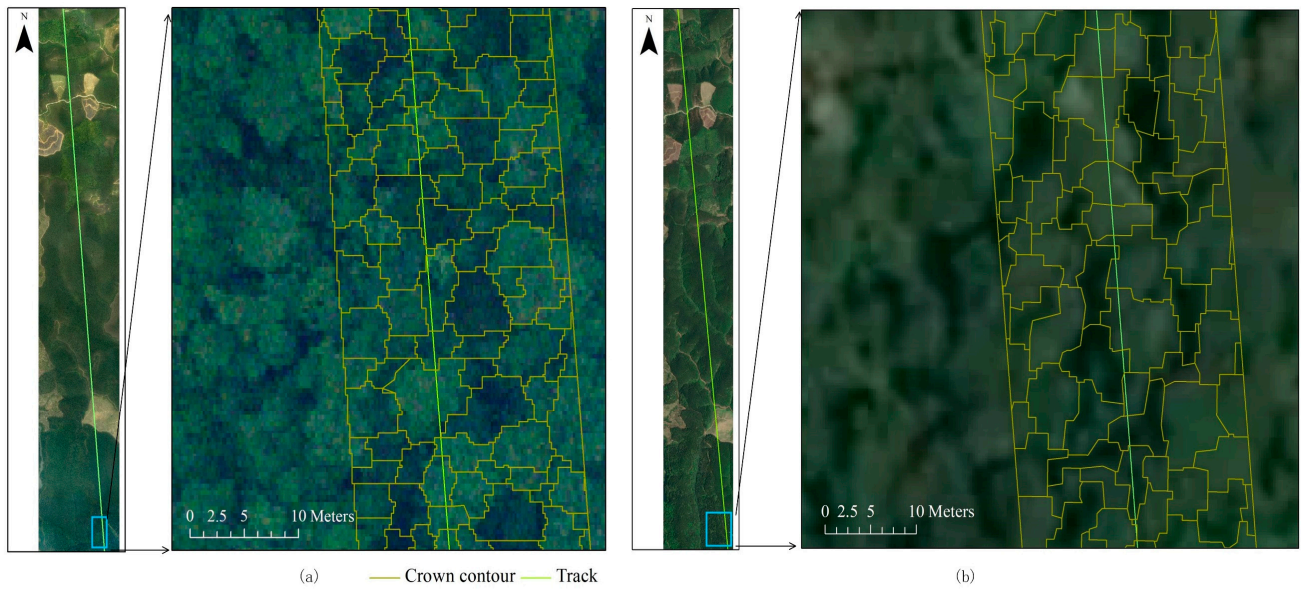
Figure 7. Example of segmentation results of the (**a**) CAF–LiCHy DOM data and (**b**) Google Earth image.

The geometric moment of the images was calculated to derive a binary map and obtain the center of mass position of the segmented object (Equation (6)), which was used as the crown center [57]. We vectorized the final segmentation results to obtain the tree crown delineations.

$$\begin{cases} x = \frac{C_{10}}{C_{00}} = \frac{\sum_{i=1}^{M}\sum_{j=1}^{N} i \cdot \varnothing^N(i,j)}{\sum_{i=1}^{M}\sum_{j=1}^{N} \varnothing^N(i,j)} \\ y = \frac{C_{01}}{C_{00}} = \frac{\sum_{i=1}^{M}\sum_{j=1}^{N} j \cdot \varnothing^N(i,j)}{\sum_{i=1}^{M}\sum_{j=1}^{N} \varnothing^N(i,j)} \end{cases} \tag{6}$$

where $\phi N(x, y)$ is the pixel value of the binary image, C_{10} is the cumulative sum of the product of the x-coordinate value of the tree canopy profile and the gray value of the image element, C_{01} is the cumulative sum of the product of the y-coordinate value of the tree canopy profile and the gray value of the image element, and C_{00} is the cumulative sum of the gray values of the canopy profile image elements.

TOC Photon Correction

The slope and slope direction parameters were calculated from the DTM derived from the ICESat–2 data. The relative positions of the TOC photons and crown center points were obtained after segmenting the high spatial resolution DOM. We used the slope, D_d, the orientation parameter, and the canopy correction rule (CCR) to eliminate the canopy height errors caused by the slope (cf. Equation (7)). If the TOC photon and the crown center point were located on the ATD, the relative distance could be calculated directly. Otherwise, the crown center point was projected onto the ATD, and the relative distance was calculated. The TOC photon locations whose D_d were greater than 0.5 m were corrected. The values were not corrected when the TOC photons were located between adjacent canopies (cf. Figure 8). The highest local canopy point was obtained by Equation (7) and represented the corrected canopy height. Due to the different crown segmentation results for the 0.2 m and 0.3 m spatial resolution images, the locations of the crown centroids were different, resulting in differences in D_d and S. The correction results obtained from the 0.3 m spatial resolution image were called CCR–1, and those based on the 0.2 m spatial resolution image were called CCR–2.

$$h_{ATLCCM} = H_{TOC} - S \cdot D_d \tan p \tag{7}$$

where h_{ATLCCM} is the canopy height after correction, H_{TOC} is the TOC photon height, D_d is the distance between the TOC photon and the center point of the crown, p is the slope,

and S is the orientation parameter. When the crown center point was located on the south slope, the TOC photon was located south relative to the crown center at $S = 1$. The TOC photon was located north relative to the crown center at $S = -1$. When the crown center point was located on the north slope, the TOC photon was located south relative to the crown center at $S = -1$, and the TOC photon was located north relative to the crown center at $S = 1$. When $D_d \leq 0.5$ m or the TOC photon was not located on the tree crown, $S = 0$. The calculations were performed in ArcGIS 10.7 and Python 3.8.
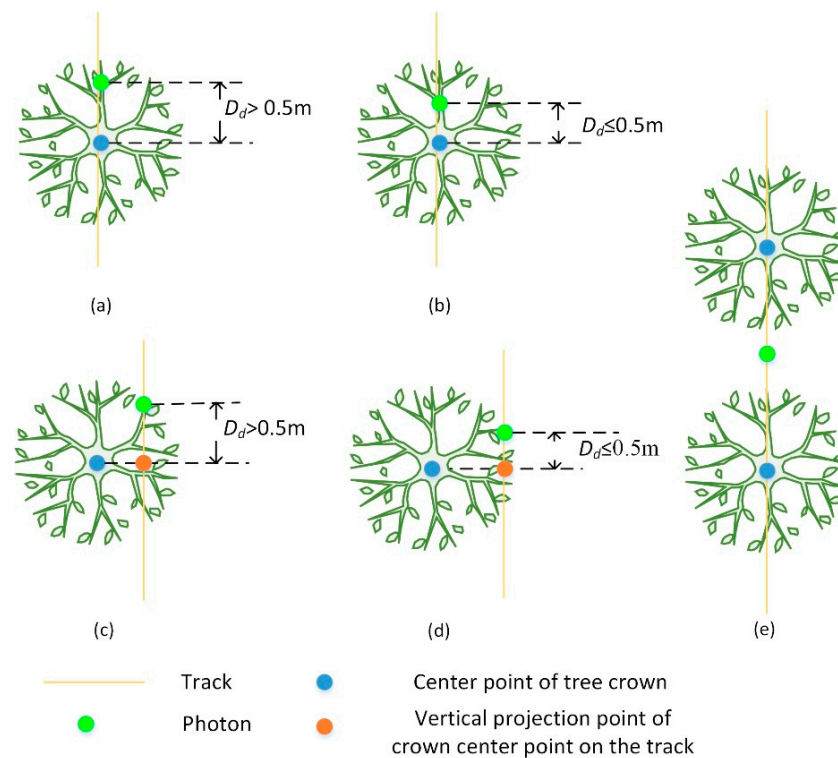
Figure 8. Schematic diagram of TOC photon correction rules: (**a**) the crown centroid and TOC photon are located in the same vertical direction and $D_d > 0.5$ m; the TOC photon is corrected; (**b**) the crown centroid and TOC photon are located in the same vertical direction, $D_d < 0.5$ m, and no correction is applied to the TOC photon; (**c**) the crown centroid and TOC photon are not in the same vertical direction, and the crown centroid is projected vertically to the orbit where the TOC photon is located. The TOC photon is corrected when the projection point to the TOC photon $D_d > 0.5$ m; (**d**) the crown centroid projection point to the TOC photon $D_d < 0.5$ m. The TOC photon is not corrected; (**e**) the TOC photons are not corrected when they are located between adjacent canopies.

2.3.5. Extraction of Canopy Parameters

The DSM and DTM were obtained by applying a third spline interpolation to the ground photons and TOC photons (cf. Figure 5d). The DTM and DSM were subtracted to obtain the CHM. The CHM was divided into 10 m, 20 m, 30 m, 40 m, 50 m, 60 m, 70 m, 80 m, 90 m, and 100 m segments in the along-track direction, and the effect of the segment size on the accuracy was compared. We calculated the relative height index for the different segments (RH70, RH75, RH80, RH85, RH90, RH95, RH98, RH100). In addition, we used the canopy relief ratio (CRR) [58,59] to analyze the canopy height differences within a 10 m segment:

$$HC_i = H_{canopy} - H_{terrain} \tag{8}$$

$$DH = \text{sort}(HC) \tag{9}$$

$$RH_j = DH(i)\ j = 70, 75, 80, 85, 90, 95, 100\ ; i = j \cdot 0.01 \cdot n \tag{10}$$

$$\text{CRR} = \frac{h_{mean} - h_{min}}{h_{max} - h_{min}} \tag{11}$$

where HC_i is the height of each vegetation point relative to the ground, H_{canopy} is the canopy elevation, $H_{terrain}$ is the ground elevation, DH is the dataset obtained by sorting the height of all vegetation points relative to the ground in ascending order, i is the number of vegetation points in the DH data $(1, 2, \ldots, n)$, j is the percent. h_{mean}, h_{min}, and h_{max} are the mean, minimum, and maximum canopy heights, respectively. CRR ranges from 0 to 1.

2.3.6. Accuracy Validation

We compared the accuracy of the forest canopy heights (CHM$_{\text{ATL08}}$, CHM$_{\text{ATL03 initial}}$, CHM$_{\text{CPTC}}$ CHM$_{\text{CCR–1}}$, and CHM$_{\text{CCR–2}}$) extracted from the ICESat–2 photon cloud data with that obtained from the CAF–LiCHy data. It has been shown that the vegetation height based on photon data is highly correlated with the 95th percentile height of conventional airborne LiDAR data [52]. Therefore, the 95th percentile height of the airborne CHM was used as the validation data to validate the accuracy of the data at the photon level and segment level. The determination coefficient (R^2), bias of mean (Bias), mean absolute error (MAE), and root mean square error (RMSE) were used to verify the accuracy of the canopy height obtained from ICESat–2 data.

R^2: Determination coefficient

$$R^2 = 1 - \frac{RMSE^2}{Var(h_{ALS})} \tag{12}$$

Bias:

$$\text{Bias} = \frac{1}{n} \sum_{i=1}^{n} (h_{ALS} - h_{ATL}) \tag{13}$$

MAE: Mean absolute error

$$\text{MAE} = \frac{1}{n} \sum_{i=1}^{n} |(h_{ALS} - h_{ATL})| \tag{14}$$

MAE': Normalized mean absolute error

$$\text{MAE}' = \frac{MAE - \min(MAE)}{\max(MAE) - \min(MAE)} \tag{15}$$

RMSE: Root Mean Square Error

$$\text{RMSE} = \sqrt{\frac{1}{n} \sum_{i=1}^{n} (h_{ALS} - h_{ATL})^2} \tag{16}$$

where h_{ALS} is the height obtained from the CAF–LiCHy data, h_{ATL} is the height obtained by inversion from the ICESat–2 data, and n is the number of total photons. MAE' is a linear transformation of the MAE to obtain values in the range of [0, 1].

3. Results

3.1. Canopy Height before and after Correction

Figure 9 shows the canopy heights from ATL08, initial ATL03, and after cross-track photon correction and canopy height correction. The canopy height provided by ATL08 is significantly overestimated in this region compared with that extracted from the CAF–LiCHy LiDAR data. The MAE and RMSE exceed 20 m. Figure 9 and Table 3 show that although ATL08 provides the canopy height per 100 m segment, there is a substantial difference between its canopy height and that obtained from the airborne LiDAR, resulting in low accuracy. These results suggest that ATL08 may not be suitable for obtaining canopy heights in subtropical forest areas.
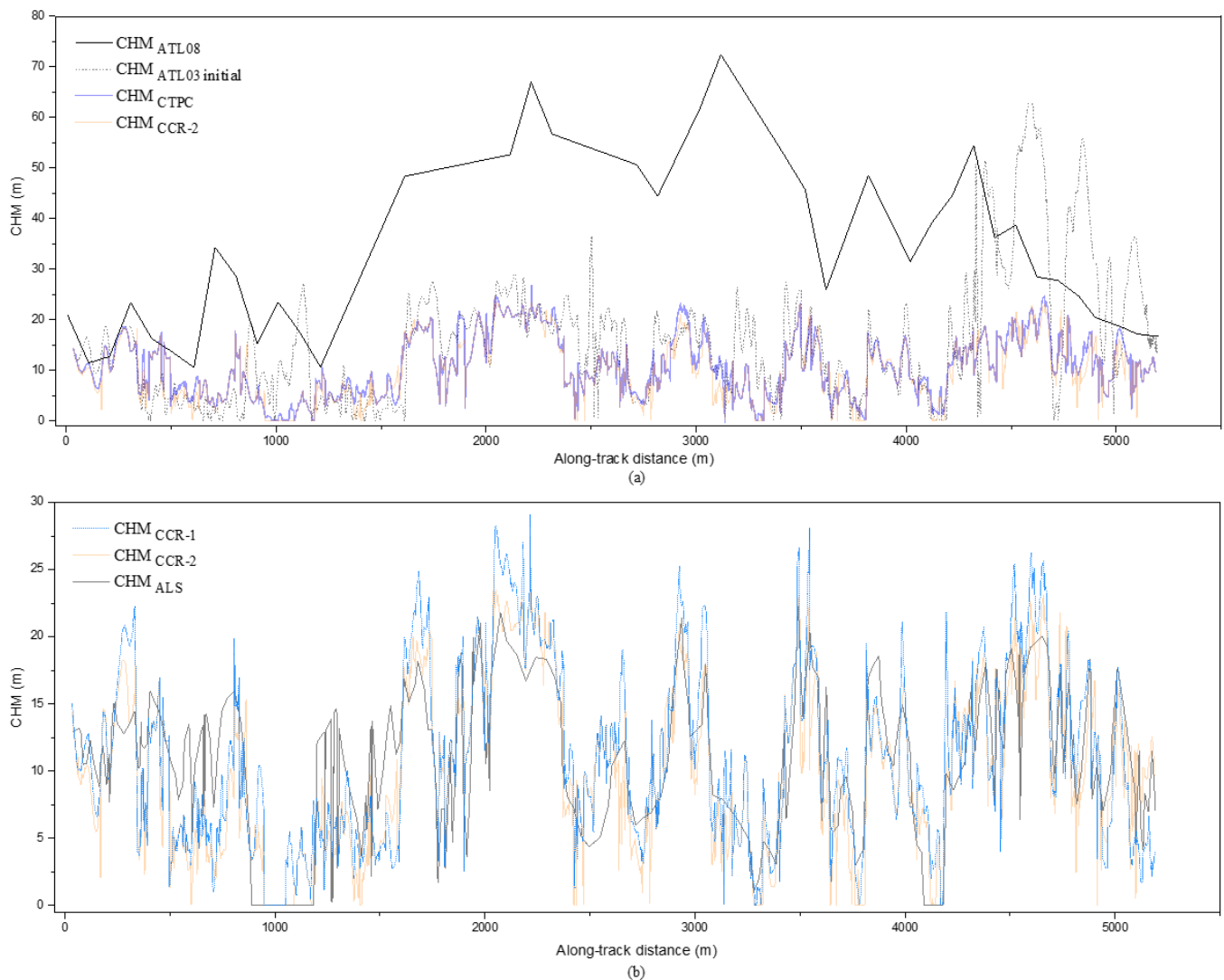
Figure 9. Comparison of airborne and spaceborne canopy height estimates retrieved by different methods: (**a**) is the result of CHM_{ATL08}, $CHM_{ATL03\ initial}$, CHM_{CTPC} and CHM_{CCR-2}, (**b**) is the result of CHM_{CCR-1}, CHM_{CCR-2} and CHM_{ALS}.

Table 3. Accuracy of tree height inversion for different methods.

	CHM_{ATL08}	$CHM_{ATL03\ initial}$	CHM_{CTPC}	CHM_{CCR-1}	CHM_{CCR-2}
R^2	0.19	0.34	0.47	0.61	0.65
Bias/(m)	22.91	1.17	1.39	1.55	−0.75
MAE/(m)	22.96	6.02	3.87	3.26	2.98
RMSE/(m)	27.68	7.31	4.68	4.08	3.78

The accuracy of $CHM_{ATL03\ initial}$ extracted by the conventional method from the ATL03 data is higher than that of CHM_{ATL08}, but the error is relatively large. After applying the cross-track photon correction before photon denoising and slope filtering for ground photon selection, the canopy height R^2 increased by 38.24%, MAE decreased by 35.71%, and the RMSE decreased by 35.98%, indicating a significant improvement in accuracy. The accuracy of canopy height estimation was further improved by applying the slope factor correction method. The MAE of CHM_{CCR-1} decreased by 15.58%, and the RMSE decreased by 12.73%. The MAE of CHM_{CCR-2} decreased by 23%, and the RMSE decreased by 19.23%. CHM_{CCR-2} showed better results than CHM_{CCR-1}. The difference between CHM_{CCR-1} and CHM_{CCR-2} was due to the different D_d

extracted from different ancillary images. As shown in Figures 9 and 10 and Table 3, the canopy height correction further reduced the canopy height error. Compared to the $CHM_{ATL03\ initial}$, the CHM_{CCR-2} improved the R^2 by 91.18% and reduced the MAE by 50.50% and the RMSE by 48.29%. The R^2 of CHM_{CCR-2} explained 65% of the variation in canopy height, indicating a significant improvement over the pre-correction estimates. The results of CHM_{CCR-1} and CHM_{CCR-2} show that the slope-based canopy correction method improves the goodness of fit and reduces the error.
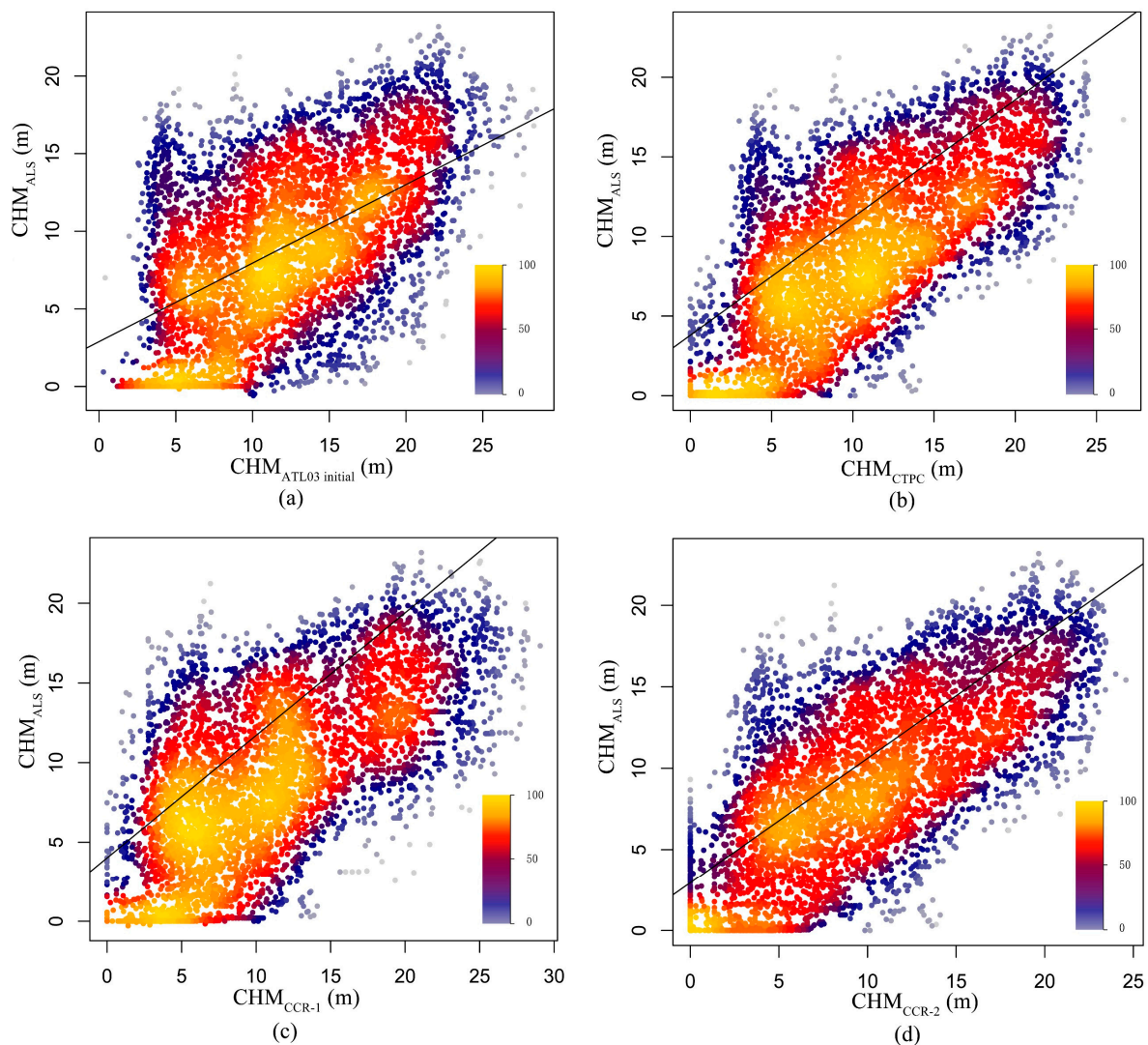
Figure 10. Scatter plot of tree heights retrieved by different methods and canopy height from CAF–LiCHy data: (**a**) uncorrected ICESat–2 tree height; (**b**) cross-track photon corrected tree height, (**c**,**d**) tree height after cross-track photon correction and TOC photon correction. The difference is that the D_d value in (**c**) is derived from the 0.3 m image, and the D_d value in (**d**) is obtained from the 0.2 m image.

3.2. Accuracy of Canopy Height Estimation for Different Segment Sizes and Relative Heights

This section describes the results of a sensitivity analysis of the forest canopy height parameters for different segment sizes and different percentile heights. Table 4 lists the canopy height accuracies before and after applying the proposed canopy height correction model for different segment sizes. The canopy height error decreases with an increase in the segment size, reaching the highest R^2 and the lowest MAE and RMSE for the 100 m segment. The larger the segment distance, the better the performance of the canopy height correction model is. As the segment size increases, the R^2 of $CHM_{ATL03\ initial}$ increases from

0.35 to 0.41, the MAE decreases from 5.94 m to 4.76 m, and the RMSE decreases from 7.17 m to 5.79 m. The R^2 of CHM_{CTPC} increases from 0.58 to 0.68, the MAE decreases from 3.29 m to 2.63 m, and the RMSE decreases from 4.03 m to 3.18 m. The R^2 of CHM_{CCR-2} increases from 0.66 to 0.74, the MAE decreases from 2.78 m to 2.10 m, and the RMSE decreases from 3.53 m to 2.72 m. The sensitivity analysis of the forest parameters shows that the MAE and RMSE of $CHM_{ATL03\ initial}$ show a rapid decrease with an increase in the segment size until 60 m, followed by a small decrease. The MAE and RMSE of CHM_{CTPC} show a rapidly decreasing trend before the 50 m segment and a small decrease afterward. The MAE and RMSE of CHM_{CCR-2} show a rapidly decreasing trend before the 40 m segment and a small decrease afterward. The proposed cross-track photon correction and canopy height correction method improve the accuracy of canopy height estimation in a small area. In addition, $CHM_{ATL03\ initial}$, CHM_{CTPC}, and CHM_{CCR-2} provide better performances than CHM_{ATL08} for the 100 m segment size.

Table 4. Inversion accuracy of uncorrected and corrected canopy heights for different segment sizes.

Datasets	Accuracy Indices	Segment Size/(m)									
		10	20	30	40	50	60	70	80	90	100
$CHM_{ATL03\ initial}$	R^2	0.35	0.36	0.38	0.39	0.40	0.40	0.40	0.40	0.42	0.41
	Bias/(m)	1.16	1.20	1.19	1.27	1.25	1.17	1.26	1.19	1.19	1.16
	MAE/(m)	5.94	5.79	5.61	5.43	5.33	5.13	5.03	5.07	4.88	4.76
	RMSE/(m)	7.17	6.96	6.70	6.57	6.35	6.08	6.03	5.89	5.85	5.79
CHM_{CTPC}	R^2	0.58	0.62	0.64	0.64	0.65	0.66	0.67	0.68	0.69	0.68
	Bias/(m)	1.39	1.39	1.39	1.39	1.40	1.39	1.40	1.40	1.40	1.40
	MAE/(m)	3.29	3.10	3.00	2.91	2.90	2.78	2.75	2.67	2.60	2.63
	RMSE/(m)	4.03	3.79	3.64	3.58	3.50	3.40	3.36	3.26	3.19	3.18
CHM_{CCR-2}	R^2	0.66	0.69	0.70	0.71	0.72	0.73	0.73	0.73	0.74	0.74
	Bias/(m)	−0.74	−0.74	−0.74	−0.74	−0.72	−0.74	−0.73	−0.72	−0.72	−0.72
	MAE/(m)	2.78	2.66	2.56	2.43	2.43	2.31	2.31	2.20	2.12	2.10
	RMSE/(m)	3.53	3.33	3.21	3.10	3.03	2.94	2.91	2.82	2.77	2.72

The percentile canopy height is crucial for describing the vertical structure of forests and modeling forest biomass. Therefore, an accuracy assessment of the percentile height was performed. Table 5 shows the sensitivity of eight percentiles of the forest canopy height at the photon level (RH70, RH75, RH80, RH85, RH90, RH95, RH98, and RH100). The R^2 range of CHM_{ATL08} is 0.17~0.19, that of $CHM_{ATL03\ initial}$ is 0.33~0.36, that of CHM_{CTPC} is 0.45~0.48, and that of CHM_{CCR-2} is 0.63~0.68. The R^2 does not change significantly with an increase in the percentile and is not shown in Table 5. The Bias, MAE, and RMSE of CHM_{ATL08} decrease with a decrease in the percentile canopy height. $CHM_{ATL03\ initial}$, CHM_{CTPC}, and CHM_{CCR-2} exhibit a decrease followed by an increase in the Bias, MAE, and RMSE with the decreasing percentile canopy height. The difference is that $CHM_{ATL03\ initial}$ reaches the minimum error at RH75, CHM_{CTPC} at RH80, and CHM_{CCR-2} at RH98. The results show that the canopy–corrected heights of CHM_{CCR-2} have the lowest errors, indicating that the proposed canopy correction method reduces the error.

Table 5. Percentile canopy heights retrieved by different methods.

Datasets	Accuracy Indices	RH70	RH75	RH80	RH85	RH90	RH95	RH98	RH100
CHM_{ATL08}	Bias/(m)	13.10	14.73	16.37	18.00	19.64	21.27	22.26	22.91
	MAE/(m)	13.60	15.12	16.64	18.19	19.76	21.36	22.31	22.96
	RMSE/(m)	16.90	18.68	20.47	22.26	24.06	25.87	26.95	27.68
$CHM_{ATL03\ initial}$	Bias/(m)	−2.43	−1.83	−1.23	−0.63	−0.03	0.57	0.93.	1.17
	MAE/(m)	4.94	4.92	4.97	5.10	5.32	5.61	5.81	6.02
	RMSE/(m)	6.08	6.07	6.14	6.30	6.53	6.82	7.03	7.31

Table 5. *Cont.*

Datasets	Accuracy Indices	RH70	RH75	RH80	RH85	RH90	RH95	RH98	RH100
CHM$_{\text{CTPC}}$	Bias/(m)	−1.79	−1.26	−0.73	−0.20	0.33	0.86	1.18	1.39
	MAE/(m)	3.40	3.31	3.29	3.34	3.46	3.64	3.77	3.87
	RMSE/(m)	4.41	4.25	4.19	4.21	4.31	4.50	4.64	4.68
CHM$_{\text{CCR−2}}$	Bias/(m)	−3.75	−3.25	−2.75	−2.25	−1.75	−1.25	−0.95	−0.75
	MAE/(m)	4.21	3.83	3.50	3.22	3.03	2.95	2.95	2.98
	RMSE/(m)	5.00	4.63	4.31	4.06	3.88	3.79	3.77	3.78

3.3. Effect of Slope on Canopy Correction

ICESat–2 was designed to overcome the disadvantages of ICESat–1 regarding the measurement error on steep slopes. However, the canopy heights estimated by ICESat–2 on different slopes reveal that the error increases with the slope. The Chinese forestry slope grading standard was used to classify the slope into six classes to quantify the influence of slope on canopy height estimation. As shown in Table 6, the R^2 of CHM$_{\text{ATL03 initial}}$, CHM$_{\text{CTPC}}$, and CHM$_{\text{CCR−2}}$ decreases as the slope increases. The MAE of each slope class for CHM$_{\text{ATL03 initial}}$ is stable at 8.41~9.94 m, and the RMSE is stable at 11.50~13.10 m, showing no changes. The MAE and RMSE of CHM$_{\text{CTPC}}$ and CHM$_{\text{CCR−2}}$ increase with the slope. The MAE of each slope class for CHM$_{\text{CTPC}}$ is stable at 2.94~4.24 m, and the RMSE is stable at 3.67~5.17 m. The MAE of each slope class for CHM$_{\text{CCR−2}}$ is stable at 2.76~3.48 m, and the RMSE is stable at 3.37~4.41 m. The MAE and RMSE of CHM$_{\text{CCR−2}}$ are on average 0.75 m and 0.84 m lower than that of CHM$_{\text{CTPC}}$, respectively.

Table 6. The influence of different slopes on the canopy height estimation accuracy.

Datasets	Accuracy Indices	Slope Classes					
		I (0° ≤ Slope < 5°)	II (5° ≤ Slope < 15°)	III (15° ≤ Slope < 25°)	IV (25° ≤ Slope < 35°)	V (35° ≤ Slope < 45°)	VI (Slope ≥ 45°)
CHM$_{\text{ATL03 initial}}$	R^2	0.43	0.36	0.28	0.24	0.19	0.15
	Bias/(m)	6.98	6.12	6.00	4.54	4.00	3.09
	MAE(m)	9.22	8.41	9.28	8.93	9.94	8.67
	RMSE(m)	10.39	11.50	12.90	13.10	12.62	11.95
CHM$_{\text{CTPC}}$	R^2	0.67	0.55	0.52	0.50	0.44	0.39
	Bias/(m)	2.05	1.79	1.84	1.27	1.06	1.18
	MAE(m)	2.97	3.53	3.79	3.79	3.97	4.24
	RMSE(m)	3.67	4.29	4.56	4.70	4.90	5.17
CHM$_{\text{CCR−2}}$	R^2	0.81	0.69	0.64	0.64	0.60	0.55
	Bias/(m)	0.74	−0.45	−0.47	−0.79	−0.95	−1.04
	MAE(m)	2.76	2.77	2.82	2.99	3.00	3.48
	RMSE(m)	3.37	3.43	3.57	3.76	3.81	4.41

The errors were lower after the cross-track photon correction and canopy height correction, indicating that these proposed methods reduced the canopy height errors due to slope. The effect of the cross-track photon correction was greater than that of the canopy height correction for reducing the error.

4. Discussion

4.1. Comparison of ICESat–2 Canopy Height Inversion Accuracy

We proposed a canopy height correction method based on the cross-track photon correction of Li et al. [47] to minimize the error caused by the slope. This correction method may not be applicable to inclined trees, whose height measurements are more complicated [60]. Figure 9a shows that the ATL08 data significantly overestimate the canopy height in this region, which is consistent with the results of Sun et al. [61] but different from those of Narine et al. [21] and Duncanson et al. [53], who found that ATL08 data underestimated canopy heights. The likely reason is that ICESat–2 uses the Landsat Vegetation Continuous Fields (VCF) product [62] to define the forest. If the average VCF canopy cover per 10 km segment is >5%, the ATL08 algorithm assumes that this segment

is forested [29]. Because land-use types have changed over the past decade, ATL08 may be using an algorithm for non-forested areas, resulting in anomalous height changes. In addition, due to the properties of the photon-counting LiDAR sensor and the ATL08 algorithm, it is possible that noisy photons were incorrectly identified as canopy or terrain photons in the 100 m segment size. This error would lead to an incorrect estimation of canopy height, especially for densely or sparsely vegetated areas [24]. Therefore, using canopy height data from ATL08 is not recommended in subtropical forest areas.

Using the 20 m segment size for photon denoising and photon classification significantly improved the canopy height estimates (Figure 9a). Streutker et al. [1] also showed that a small segment size is preferable for canopy photon selection. However, a smaller segment size is not necessarily better. A lower density of the photon cloud of the vegetation signal in small segments may classify the vegetation signal as noise photons. Compared to CHM_{CTPC} and CHM_{CCR-2}, the canopy height of $CHM_{ATL03\ initial}$ was significantly overestimated, probably due to noise near the ground or at the top of the canopy after photon denoising. This noise was removed by cross-track photon correction and SFMB filtering. CHM_{CCR-2} is based on the cross-track photon correction results and introduces a slope factor to correct the TOC photons. Compared with CHM_{CTPC}, the MAE of CHM_{CCR-2} is reduced by 0.87 m and the RMSE is reduced by 0.90 m. The average correction value of TOC photons is 0.66 m. The reduced error of CHM_{CCR-2} is close to the average correction value of TOC photons. In areas with slope > 15°, TOC photon correction reduces MAE by 0.76~0.97 m and RMSE by 0.76~1.09 m. R^2 improves by 0.18 after TOC photon correction, it reflects that the canopy correction method proposed in this paper can reduce the canopy height estimation error caused by slope. CHM_{CTPC} without TOC photon correction had the lowest error at RH80. CHM_{CCR-2} with TOC photon correction had the lowest forest canopy height MAE and RMSE at RH98. It indicates that the TOC photon correction method eliminates the error caused by slope and restored the natural morphology of the forest canopy.

The ATL08 algorithm is suitable for global data processing, resulting in high errors in some regions. However, the canopy height estimates were improved after cross-track photon correction and canopy height correction based on ATL03 data, indicating that ICESat–2 could perform canopy height inversion in subtropical regions.

4.2. Influencing Factors of ICESat–2 CHM Inversion

This section describes the effects of cross-track photon correction, slope, segment size, percentile canopy height, D_d, canopy density, canopy relief rate, growth, and harvesting on canopy height estimation using ICESat–2 data.

The effect of slope on the ICESat–2 canopy height estimation is reflected in two aspects. First, if the 3D photon data are converted into 2D photon profiles without cross-track photon correction [47], errors will occur in the DTM and DSM due to the slope influence; this problem is called the horizontal error. Second, the position of the trunk bottom may be overestimated or underestimated in the vertical direction (cf. Figure 6), which is called the vertical error. Li et al. [47] reported that the MAE and RMSE of the height value in the DTM were reduced after cross-track photon correction by 1.86~2.52 m and 2.12~2.50 m, respectively. The slope can affect the canopy height estimates obtained from the DTM, resulting estimates inaccurate. The relative canopy height is the height of the canopy photons minus the height of the fitted ground. Thus, on high slopes, the errors of the ground points are transferred to the canopy height estimates. As shown in Table 3, the MAE and RMSE of the canopy heights after cross-track photon correction were reduced by 2.15 m and 2.63 m, respectively, which is similar to the improvement in the DTM accuracy by cross-track photon correction. These results show that the cross-track photon correction method not only effectively improves the ground estimation accuracy but also the canopy height estimation accuracy. After the TOC photon correction, the MAE was further reduced by 0.89 m, and the RMSE was further reduced by 0.90 m, suggesting that the horizontal

error is larger than the vertical error and that accurate terrain estimation is crucial for deriving canopy heights.

In mountainous regions, terrain undulations cause substantial uncertainty in canopy height estimation [63]. We quantified the error in the vertical direction caused by the slope. Figure 11a shows the influence of the slope on the absolute correction value. On south-facing slopes, the difference was negative when the TOC photons were north of the canopy centroid and positive when they were south of the canopy centroid. The opposite is true for north-facing slopes. The difference between the CHMs before and after correction ranged from -2.55 m to 2.90 m. A tree canopy is typically symmetrical with the trunk as the axis, and the positive and negative correction values are determined by the relative positions. Here, the correction values are the absolute values to depict the effect of slope on canopy correction. As the slope becomes steeper, the absolute correction value increases. On slopes $\leq 10°$, the absolute correction values are less than 0.50 m, indicating that the canopy height correction method is not required in low-slope areas. As shown in Table 6, the canopy heights estimated after cross-track photon correction had relatively high accuracy in flat areas. The absolute correction values are different for the same slope values due to the difference in D_d. Moreover, the fitted curve in Figure 11a shows that the vertical error increases exponentially with the slope. Therefore, the effect of the topographic slope must be considered in very steep areas. Future studies should evaluate the empirical equation of the slope correction method for ICESat–2 canopy height estimate under different environments.
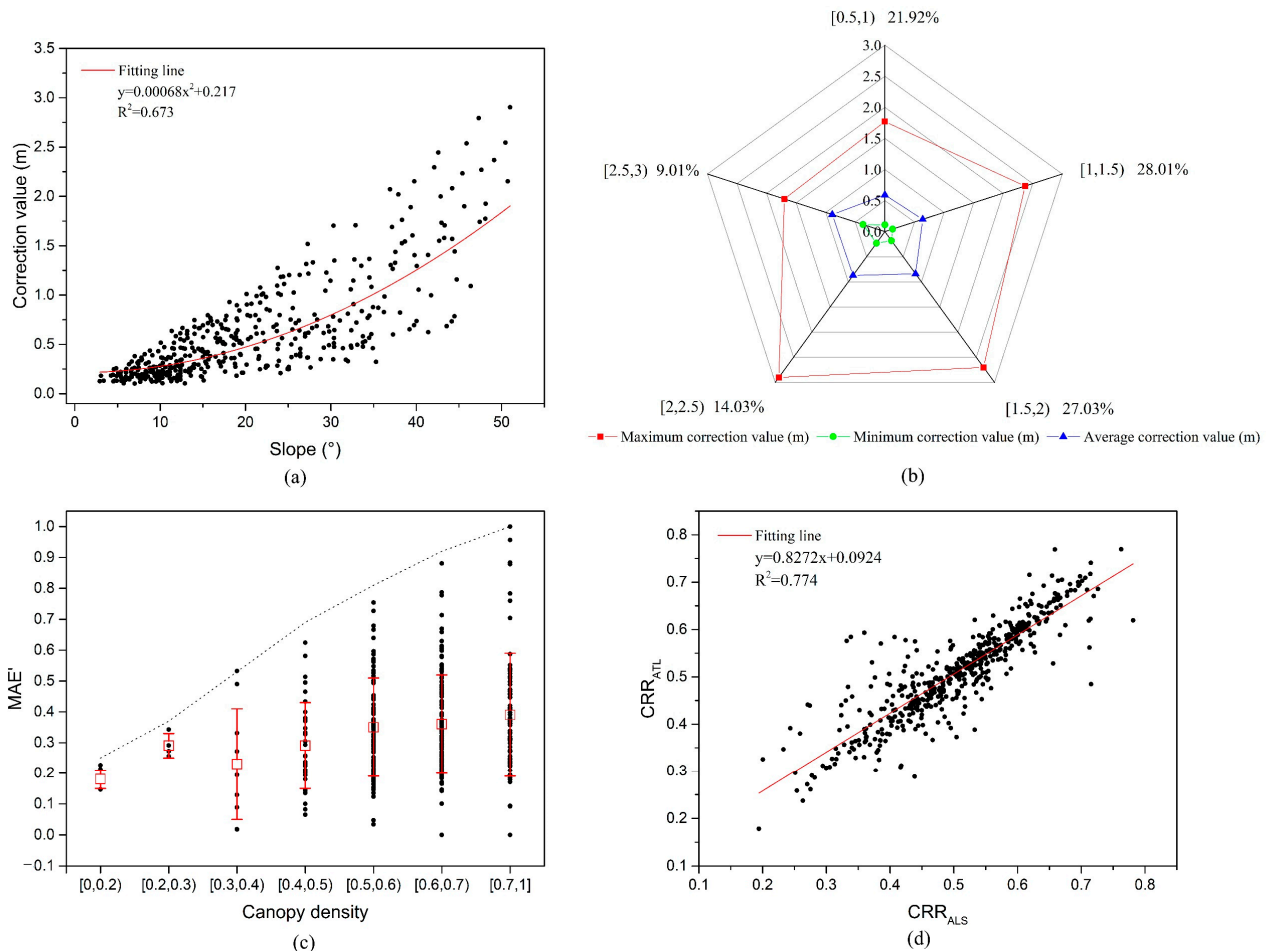
Figure 11. Analysis of influencing factors of ICESat–2 canopy height inversion: (**a**) effect of slope on the corrected canopy height; (**b**) effect of Dd on the corrected canopy height; (**c**) MAE for different canopy densities; (**d**) scatterplot of the CRR obtained from CAF–LiCHy and ICESat–2 data.

It is necessary to meet certain accuracy requirements for smaller segment sizes considering the future demand for forest parameters. We compared the sensitivity of the forest parameters for 10 segment sizes (10 m to 100 m) (cf. Table 4). The accuracy increases with an increase in the segment length, in agreement with the findings of Streutker et al. [1]. It is expected that the MAE and RMSE will continue to decrease as the segment size increases but at a slower rate. The R^2 was 0.64, and the RMSE was 3.64 m for the 30 m segment size after cross-track photon correction. Our R^2 and RMSE values were slightly smaller than those of Zhu et al. (0.70 and 4.31 m, respectively [64]. After the cross-track photon correction and canopy height correction, the R^2 was 0.70, and the RMSE was 3.21 m, better than the results of Zhu et al. [64]. The experimental results show that the combination of cross-track photon correction and canopy height correction substantially reduces the canopy height estimation error due to slope for ICESat–2 data.

A comparison of the different percentile canopy heights showed that the corrected values were more accurate than the uncorrected values, and the MAE and RMSE were the lowest at RH98. The forest canopy height results without cross-track photon correction and TOC photon correction were optimal at RH75, consistent with the findings of Neuenschwander and Pitts [29]. The forest canopy height results with cross-track photon correction were optimal at RH80. This finding indicates that canopy height correction can reduce the uncertainty in selecting the optimal percentile canopy height for different terrain conditions.

Figure 11b shows the proportions of the intervals for $D_d = 0.50$ m and the maximum, average, and minimum corrected heights. The TOC photon selection algorithm and the crown segmentation algorithm affect D_d. The highest point or percentile methods are typically used for TOC photon selection [19,20,26,28,33], and the obtained TOC photon results are relatively fixed. The canopy segmentation results depend on the tree species, canopy width, canopy morphology, planting density, solar position, and shading. The segmentation procedure is dependent on the user-specified parameters (scale, shape ratio, and compactness ratio). When trees are grouped closely together in dense stands, the ends of their branches may touch the crowns of nearby trees, resulting in larger crowns [65]. Thus, the crown centroids may have errors, which are transferred to D_d, leading to uncertainty in canopy height correction. This problem causes the largest uncertainty in the proposed canopy correction method. It is expected that crown segmentation algorithms will be improved using deep learning and other methods, minimizing this problem. Figure 11b shows that the proportion of $D_d < 2.0$ m accounts for 76.96%, which is attributed to the canopy width of 4.0~8.0 m in this area. The maximum correction value does not occur in the interval with the maximum D_d. Equation (7) indicates that the error is caused by the slope. This result suggests that the effect of slope on canopy height is not negligible, and the larger the slope, the larger the D_d is, and the larger the canopy height error is.

Figure 11c shows the normalized MAE of CHM_{CCR-2} at different canopy densities. The dashed line is the boundary line of normalized MAE at different canopy densities. Zhu et al. [34] also found that forest canopy density substantially affected the inversion of canopy height from ICESat–2 data. We classified the canopy density into seven classes to investigate the canopy density effect on the canopy height estimates of ICESat–2 data. The mean normalized MAE increased with increasing canopy density, in agreement with the results of Narine [21], Neuenschwander and Magruder [24], and Martin [66]. This study differs from others in that the MAE was not always high in areas with high canopy density, but the uncertainty of the normalized MAE rose with the increasing canopy density. The boundary line shows the maximum error of the seven canopy density classes, indicating an increasing trend of the normalized MAE. Although there is some uncertainty in this line, it highlights the differences in the error for each canopy density class, an approach rarely used in data analysis.

Existing studies on extracting forest vegetation parameters from photon-counting LiDAR data have mostly focused on canopy height inversion. Canopy height is a crucial parameter. Our study with ICESat–2 data only considered the canopy segments but not

the internal canopy characteristics, and a CHM cannot describe the canopy geometry. Therefore, we used the CRR to analyze the geometric characteristics of the tree crowns to obtain a macroscopic description of the canopy height characteristics. Because CHM_{CCR-2} provided better performance than CHM_{CCR-1}, this section compares the CRR of CHM_{CCR-2} and CHM_{ALS}. The CRR of the spaceborne LiDAR data was significantly correlated with the airborne LiDAR data, with a Pearson correlation coefficient of 0.88 and an R^2 of 0.77 (cf. Figure 11d). This result shows that the CHM derived from the spaceborne LiDAR data and the airborne LiDAR data are similar in terms of canopy characteristics. The CRR is not related to the accuracy of the ICESat–2 inversion of canopy height but indicates that the ICESat–2 CHM is relatively accurate. The CRR can be used as an index to demonstrate the accuracy of ICESat–2 data for characterizing the canopy in addition to other accuracy metrics (MAE, RMSE, etc.).

There was a difference in the acquisition time between the spaceborne LiDAR data and the airborne LiDAR data. The airborne LiDAR data were collected in April 2018, and the ICESat–2 data were collected in October 2019; thus, an exact match in time was impossible. During the one-and-a-half-year period, the trees grew, and their height changed, leading to errors. In addition, this area is an operational forest, where logging operations occur, resulting in height estimation errors. Tree planting in non-forested areas can also cause errors in canopy height estimation. Vegetation planting, growth, and harvesting affect the accuracy of forest canopy height estimation.

4.3. Future Directions and Implications

Forest height indicators extracted from ICESat–2 data have been used as critical variables for estimating biomass [21,53,67]. Our results suggest that using ICESat–2 canopy height indicators is more challenging in stands with complex terrain and high variability in canopy density. In contrast, cross-track photon correction and canopy height correction can improve the accuracy of canopy height estimates.

The findings of this study show that ICESat–2 data can be used successfully to assess the structure and characteristics of forest stands with different canopy heights, enabling large-scale monitoring and management. The results obtained from the Google Earth satellite images show the potential of their use for validation in different regions. Martin et al. [68] detected more than 1.8 billion trees in the Sahara, Sahel, and sub-humid zone of West Africa using high-resolution satellite images and depth learning algorithms. Although this method was applied to savanna areas, forest canopy segmentation on a global scale will become a reality with the development of ultra-high spatial resolution satellites and single-tree identification algorithms. Canopy correction methods will be further improved. Any single detection system has some limitations. Thus, combining different ultra-high spatial resolution satellite images (Worldview–2/3, GeoEye–1, etc.) with ICESat–2 data can be advantageous. This study demonstrates the capacity to utilize these data for estimating forest attribute values and provides a thorough review of extracting forest structure parameters from ICESat–2 data. Nie et al. [69] developed a theoretical model to quantify the effects of terrain slope, canopy radius, canopy shape, and offset distance to the slope on canopy height displacement in ellipsoidal canopies. The effect of slope on canopy height estimation may differ for different types of canopies and terrain. This paper proposes a theoretical approach to eliminating slope errors. In the future, we can build on this theory to verify the effect of different canopy shapes on canopy height estimation experimentally. ICESat–2 will be integrated with other datasets to extract detailed estimates of forest inventory parameters for monitoring purposes on a continuous time scale. This strategy is applicable due to the growing availability of ICESat–2 data and the improved capabilities for forest monitoring.

5. Conclusions

Canopy height inversion from ICESat–2 laser altimetry data is substantially influenced by slope, canopy density, and signal-to-noise ratio. Studies have shown that slope is the

most influential factor. Our results indicate that the vertical error increases exponentially with the increasing slope; thus, the effect of slope on canopy height estimation must be considered. This study proposed the first ICESat–2 CCR based on high spatial resolution DOM. The effect of slope on the canopy height estimates obtained from ICESat–2 data was minimized by the cross-track photon correction method. This method reduced the MAE by 35.71% and the RMSE by 35.98%. The canopy correction method based on high spatial resolution DOM based on the cross-track photon correction resulted in a further 23% reduction in the MAE and a 19.23% reduction in the RMSE. The proposed method significantly improved the accuracy of ICESat–2 forest canopy height estimation compared with the traditional method. Using uncorrected canopy height data from ATL08 is not recommended in subtropical forest areas.

This study investigated the sources of slope error and their effect on canopy height estimation and proposed a slope error correction method. The method is suitable for spaceborne photon-counting LiDAR systems and improves the accuracy of canopy height estimation. However, the correction method uses multi-source data, increasing the computational complexity. Thus, the method is more time-consuming than using ATL08 data for large photon point clouds. Since we focused on a theoretical approach to minimize slope errors, we did not quantify the effect of canopy morphology on canopy height estimation. Future studies will focus on the validation of our theoretical approach in different regions and ecosystems to demonstrate the applicability of the methodology.

Author Contributions: Conceptualization and methodology, B.L.; data curation, Y.Y.; data curation and data processing, B.L., W.Z. and Z.D.; original draft preparation, B.L.; paper review and editing, X.S. and G.F.; project administration and funding acquisition, T.Z. All authors have read and agreed to the published version of the manuscript.

Data Availability Statement: Not applicable.

Conflicts of Interest: The authors declare no conflict of interest.

References

1. Streutker, D.R.; Glenn, N.F. LiDAR measurement of sagebrush steppe vegetation heights. *Remote Sens. Environ.* **2006**, *102*, 135–145. [CrossRef]
2. Nie, S.; Wang, C.; Zeng, H.; Xi, X.; Xia, S. A revised terrain correction method for forest canopy height estimation using ICESat/GLAS data. *ISPRS J. Photogramm.* **2015**, *108*, 183–190. [CrossRef]
3. Fayad, I.; Baghdadi, N.; Bailly, J.S.; Barbier, N.; Gond, V.; Herault, B.; Hajj, M.E.; Fabre, F.; Perrin, J. Regional Scale Rain–Forest Height Mapping Using Regression–Kriging of Spaceborne and Airborne LiDAR Data: Application on French Guiana. *Remote Sens.* **2016**, *8*, 240. [CrossRef]
4. Schimel, D.; Pavlick, R.; Fisher, J.B.; Asner, G.P.; Saatchi, S.; Townsend, P.; Miller, C.; Frankenberg, C.; Hibbard, K.; Cox, P. Observing terrestrial ecosystems and the carbon cycle from space. *Glob. Chang. Biol.* **2015**, *21*, 1762–1776. [CrossRef]
5. Tao, S.; Guo, Q.; Li, C.; Wang, Z.; Fang, J. Global patterns and determinants of forest canopy height. *Ecology* **2016**, *97*, 3265–3270. [CrossRef]
6. Malambo, L.; Popescu, S.C. Assessing the agreement of ICESat–2 terrain and canopy height with airborne lidar over US ecozones. *Remote Sens. Environ.* **2021**, *266*, 112711. [CrossRef]
7. Wulder, M.A.; Bater, C.W.; Coops, N.C.; Hilker, T.; White, J.C. The role of LiDAR in sustainable forest management. *For. Chron.* **2008**, *84*, 807–826. [CrossRef]
8. Wulder, M.A.; White, J.C.; Nelson, R.F.; Naesset, E.; Orka, H.O.; Coops, N.C.; Hilker, T.; Bater, C.W.; Gobakken, T. LiDAR sampling for large–area forest characterization: A review. *Remote Sens. Environ.* **2012**, *121*, 196–209. [CrossRef]

9.   White, J.C.; Coops, N.C.; Wulder, M.A.; Vastaranta, M.; Hilker, T.; Tompalski, P. Remote sensing Technologies for Enhancing Forest Inventories: A review. *Can. J. Remote Sens.* **2016**, *42*, 619–641. [CrossRef]

10. Scott, C.P.; Phan, M.; Crosby, C.J.; Nandigam, V.; Arrowsmith, R. On–demand 3D topographic differencing hosted by open topography. In Proceedings of the AGU Fall Meeting Abstracts 2019 (AGUFM 2019), San Francisco, CA, USA, 9–13 December 2019.

11. Thatcher, C.A.; Lukas, V.; Stoker, J.M. *The 3D Elevation Program and Energy for the Nation*; US Geological Survey: Reston, VA, USA, 2020.

12. Narine, L.L.; Popescu, S.C.; Malambo, L. Using ICESat–2 to estimate and map forest aboveground biomass: A first example. *Remote Sens.* **2020**, *12*, 1824. [CrossRef]

13. Neumann, T.A.; Martino, A.J.; Markus, T.; Bae, S.; Bock, M.R.; Brenner, A.C.; Brunt, K.M.; Cavanaugh, J.; Fernandes, S.T.; Hancock, D.W.; et al. The Ice, Cloud, and Land Elevation Satellite–2 mission: A global geolocated photon product derived from the Advanced Topographic Laser Altimeter System. *Remote Sens. Environ.* **2019**, *233*, 111325. [CrossRef] [PubMed]

14. Degnan, J.J. Scanning, multibeam, single photon lidars for rapid, large scale, high resolution, topographic and bathymetric mapping. *Remote Sens.* **2016**, *8*, 958. [CrossRef]

15. Magruder, L.A.; Brunt, K.M.; Alonzo, M. Early ICESat–2 on–orbit Geolocation Validation Using Ground–Based Corner Cube Retro–Reflectors. *Remote Sens.* **2020**, *12*, 3653. [CrossRef]

16. Harding, D.J.; Dabney, P.W.; Valett, S. Polarimetric, two–color, photon–counting laser altimeter measurements of forest canopy structure. In *International Symposium on Lidar and Radar Mapping 2011: Technologies and Applications*; International Society for Optics and Photonics: San Diego, CA, USA, 2011; p. 828629.

17. Zhu, X.; Nie, S.; Wang, C.; Xi, X.B.; Li, D.; Li, G.Y.; Wang, P.; Cao, D.; Yang, X.B. Estimating Terrain Slope from ICESat–2 Data in Forest Environments. *Remote Sens.* **2020**, *12*, 3300. [CrossRef]

18. Lin, X.; Xu, M.; Cao, C.; Dang, Y.; Huang, Z. Estimates of forest canopy height using a combination of ICESat–2/atlas data and stereo–photogrammetry. *Remote Sens.* **2020**, *12*, 3649. [CrossRef]

19. Gwenzi, D.; Lefsky, M.A.; Suchdeo, V.P.; David, J.H. Prospects of the ICESat–2 laser altimetry mission for savanna ecosystem structural studies based on airborne simulation data. *ISPRS J. Photogramm.* **2016**, *118*, 68–82. [CrossRef]

20. Popescu, S.C.; Zhou, T.; Nelson, R.; Neuenschwander, A.; Sheridan, R.; Narine, L.; Walsh, K.M. Photon counting LiDAR: An adaptive ground and canopy height retrieval algorithm for ICESat–2 data. *Remote Sens. Environ.* **2018**, *208*, 154–170. [CrossRef]

21. Narine, L.L.; Popescu, S.; Neuenschwander, A.; Zhou, T.; Srinivasan, S.; Harbeck, K. Estimating aboveground biomass and forest canopy cover with simulated ICESat–2 data. *Remote Sens. Environ.* **2019**, *224*, 1–11. [CrossRef]

22. Neuenschwander, A.; Guenther, E.; White, J.C.; Duncanson, L.; Montesano, P. Validation of ICESat–2 terrain and canopy heights in boreal forests. *Remote Sens. Environ.* **2020**, *251*, 112110. [CrossRef]

23. Liu, A.; Cheng, X.; Chen, Z. Performance evaluation of GEDI and ICESat–2 laser altimeter data for terrain and canopy height retrievals. *Remote Sens. Environ.* **2021**, *264*, 112571. [CrossRef]

24. Neuenschwander, A.L.; Magruder, L.A. Canopy and Terrain Height Retrievals with ICESat–2: A First Look. *Remote Sens.* **2019**, *11*, 1721. [CrossRef]

25. Wang, Y.; Wang, H.; Li, S.; Zhou, H. Error analysis of estimated canopy height based on photon counting laser altimetry. *Infrared Laser Eng.* **2021**, *40*, 223–229.

26. Moussavi, M.S.; Abdalati, W.; Scambos, T.; Neuenschwander, A. Applicability of an automatic surface detection approach to micro–pulse photon–counting lidar altimetry data: Implications for canopy height retrieval from future ICESat–2 data. *Int. J. Remote Sens.* **2014**, *35*, 5263–5279. [CrossRef]

27. Kwok, R.; Markus, T.; Morison, J.; Palm, S.P.; Neumann, T.A.; Brunt, K.M.; Cook, W.B.; Hancock, D.W.; Cunningham, G.F. Profiling Sea Ice with a Multiple Altimeter Beam Experimental Lidar (MABEL). *J. Atmos. Ocean Technol.* **2014**, *31*, 1151–1168. [CrossRef]

28. Nie, S.; Wang, C.; Xi, X.; Luo, S.Z.; Li, G.Y.; Tian, J.Y.; Wang, H.G. Estimating the vegetation canopy height using micro–pulse photon–counting LiDAR data. *Opt. Express* **2018**, *26*, 520–540. [CrossRef]

29. Neuenschwander, A.; Pitts, K. The ATL08 land and vegetation product for the ICESat–2 Mission. *Remote Sens. Environ.* **2019**, *221*, 247–259. [CrossRef]

30. Wang, C.; Zhu, X.; Nie, S.; Xi, X.; Li, D.; Zheng, W.; Chen, S. Ground elevation accuracy verification of ICESat–2 data: A case study in Alaska, USA. *Opt. Express* **2019**, *27*, 38168–38179. [CrossRef]

31. Takahashi, T.; Yamamoto, K.; Senda, Y.; Tsuzuku, M. Estimating individual tree heights of sugi (Cryptomeria japonica D. Don) plantations in mountainous areas using small–footprint airborne LiDAR. *J. For. Res.* **2005**, *10*, 135–142. [CrossRef]

32. Hodgson, M.E.; Bresnahan, E. Accuracy of airborne LiDAR–derived elevation: Empirical assessment and error budget. *Photogramm. Eng. Remote Sens.* **2004**, *70*, 331–339. [CrossRef]

33. Zhu, X.; Nie, S.; Wang, C.; Xi, X.H.; Hu, Z.Y. A Ground Elevation and Vegetation Height Retrieval Algorithm Using Micro–Pulse Photon–Counting Lidar Data. *Remote Sens.* **2018**, *10*, 1962. [CrossRef]

34. Wang, L.X.; Zhou, H.; Li, Z.L.; Liu, G.G.; Wang, H.; Wang, Y.P. Simulation of terrestrial target response function for satellite laser altimeter. *Infrared Laser Eng.* **2015**, *34*, 3424–3430.

35. Zhang, Z.Y.; Wang, H.; Zhang, W.H.; Huang, K.; Zhou, H.; Ma, Y.; Li, S. Semi–analytical model of the waveform of plantation target for a satellite laser altimater. *Acta Geod. Cartogr. Sin.* **2018**, *47*, 142–152.

36. Ni, X.; Xu, M.; Cao, C.; Chen, W.; Yang, B.; Xie, B. Forest height estimation and change monitoring based on artificial neural network using Geoscience Laser Altimeter System and Landsat data. *J. Appl. Remote Sens.* **2019**, *14*, 022207. [CrossRef]
37. Martino, A.; Bock, M.R.; Jones, R.L.; Neumann, T.A.; Hancock, D.W.; Dabney, P.W.; Webb, C.E. The Ice, Cloud and Land Elevation Satellite–2 Project: Algorithm Theoretical Basis Document (ATBD)for ATL02 (Level 1B) Data Product, NASA Tech. Document, ICESat–2–SIPS–SPEC–0150. Available online: https://ICESat--2.gsfc.nasa.gov/sites/default/files/page_files/ICESat2_ATL02_ATBD_r003.pdf (accessed on 23 November 2020).
38. Li, S.; Zhang, Z.; Ma, Y.; Zeng, H.M.; Zhao, P.F.; Zhang, W.H. Ranging performance models based on negative–binomial (NB) distribution for photon–counting lidars. *Opt. Express* **2019**, *27*, 861–877. [CrossRef] [PubMed]
39. Magruder, L.A.; Brunt, K.M. Performance Analysis of Airborne Photon–Counting Lidar Data in Preparation for the ICESat–2 Mission. *IEEE Trans. Geosci. Remote* **2018**, *56*, 2911–2918. [CrossRef]
40. Tadono, T.; Ishida, H.; Oda, F.; Naito, S.; Minakawa, K.; Iwamoto, H. Precise global DEM generation by ALOS PRISM. *ISPRS Ann. Photogramm. Remote Sens. Spat. Inf. Sci.* **2014**, *2*, 71–76. [CrossRef]
41. Shebl, A.; Csámer, A. Reappraisal of DEMs, Radar and optical datasets in lineaments extraction with emphasis on the spatial context. *Remote Sens. Appl. Soc. Environ.* **2021**, *24*, 100617. [CrossRef]
42. Lu, D.S.; Chen, Q.; Wang, G.X.; Liu, L.J.; Li, G.Y.; Moran, E. A survey of remote sensing–based aboveground biomass estimation methods in forest ecosystems. *Int. J. Digit. Earth* **2014**, *9*, 63–105. [CrossRef]
43. Ma, L.X.; Zheng, G.; Eitel, J.U.H.; Magney, T.S.; Moskal, L.M. Retrieving forest canopy extinction coefficient from terrestrial and airborne LiDAR. *Agric. For. Meteorol.* **2017**, *236*, 1–21. [CrossRef]
44. Falkowski, M.J.; Wulder, M.A.; White, J.C.; Gillis, M.D. Supporting large–area, sample–based forest inventories with very high spatial resolution satellite imagery. *Prog. Phys. Geog.* **2009**, *33*, 403–423. [CrossRef]
45. Pang, Y.; Li, Z.Y.; Ju, H.B.; Lu, H.; Jia, W.; Si, L.; Guo, Y.; Liu, Q.W.; Li, S.M.; Liu, L.X.; et al. LiCHy: The CAF's LiDAR, CCD and Hyperspectral Integrated Airborne Observation System. *Remote Sens.* **2016**, *8*, 398. [CrossRef]
46. Nie, S.; Wang, C.; Dong, P.; Xi, X.; Luo, S.; Qin, H. A revised progressive TIN densification for filtering airborne LiDAR data. *Measurement* **2017**, *104*, 70–77. [CrossRef]
47. Li, B.; Fan, G.P.; Zhao, T.Z.; Deng, Z.; Yu, Y.H. Retrieval of DTM under Complex Forest Stand Based on Spaceborne LiDAR Fusion Photon Correction. *Remote Sens.* **2022**, *14*, 218. [CrossRef]
48. Tian, X.; Shan, J. Comprehensive Evaluation of the ICESat–2 ATL08 Terrain Product. *IEEE Trans. Geosci. Remote* **2021**, *99*, 1–15. [CrossRef]
49. Fu, H.; Zhu, J.; Wang, C.; Wang, H.; Zhao, R. Underlying topography estimation over forest areas using high–resolution p–band single–baseline polinsar data. *Remote Sens.* **2017**, *9*, 363. [CrossRef]
50. Herzfeld, U.C.; McDonald, B.W.; Wallin, B.F.; Neumann, T.A.; Markus, T.; Brenner, A.; Fileld, C. Algorithm for detection of ground and canopy cover in micropulse photon–counting Lidar altimeter data in preparation for the ICESat–2 mission. *IEEE Trans. Geosci. Remote Sens.* **2014**, *52*, 2109–2125. [CrossRef]
51. Duan, Z.G.; Zhao, D.; Zeng, Y.; Zhao, Y.J.; Wu, B.F.; Zhu, J.J. Assessing and Correcting Topographic Effects on Forest Canopy Height Retrieval Using Airborne LiDAR Data. *Sensors* **2015**, *15*, 12133–12155. [CrossRef]
52. Neuenschwander, A.N.; Magruder, L.M. The Potential Impact of Vertical Sampling Uncertainty on ICESat–2/ATLAS Terrain and Canopy Height Retrievals for Multiple Ecosystems. *Remote Sens.* **2016**, *8*, 1039. [CrossRef]
53. Duncanson, L.; Neuenschwander, A.; Hancock, S.; Thomas, N.; Fatoyinbo, T.; Simard, M.; Silva, C.A.; Armston, J.; Scott, B. Biomass estimation from simulated GEDI, ICESat–2 and NISAR across environmental gradients in sonoma county, california. *Remote Sens. Environ.* **2020**, *242*, 111779. [CrossRef]
54. Chen, Y.; Chen, Q.; Jing, C. Multi–resolution segmentation parameters optimization and evaluation for VHR remote sensing image based on mean NSQI and discrepancy measure. *J. Spat. Sci.* **2019**, *66*, 1–26.
55. Roth, K.L.; Roberts, D.A.; Dennison, P.E.; Peterson, S.H.; Alonzo, M. The impact of spatial resolution on the classification of plant species and functional types within imaging spectrometer data. *Remote Sens. Environ.* **2015**, *171*, 45–57. [CrossRef]
56. Skurikhin, A.N.; Garrity, S.R.; McDowell, N.G.; Dongming, M. Automated tree crown detection and size estimation using multi–scale analysis of high–resolution satellite imagery. *Remote Sens. Lett.* **2013**, *4*, 465–474. [CrossRef]
57. Dong, X.Y.; Li, J.G.; Chen, H.Y.; Zhao, L.; Zhang, L.M.; Xing, S.H. Extraction of individual tree information based on remote sensing images from an Unmanned Aerial Vehicle. *J. Remote Sens.* **2019**, *23*, 1269–1280.
58. Parker, G.G.; Russ, M.E. The canopy surface and stand development: Assessing forest canopy structure and complexity with near–surface altimetry. *For. Ecol. Manag.* **2004**, *189*, 307–315. [CrossRef]
59. Chirici, G.; McRoberts, R.E.; Fattorini, L.; Mura, M.; Marchetti, M. Comparing echo–based and canopy height model–based metrics for enhancing estimation of forest aboveground biomass in a model–assisted framework. *Remote Sens. Environ.* **2016**, *174*, 1–9. [CrossRef]
60. Gatziolis, D.; Fried, J.S.; Monleon, V.S. Challenges to estimating tree height via LiDAR in closed–canopy forests: A parable from western Oregon. *For. Sci.* **2010**, *56*, 139–155.
61. Sun, T.; Qi, J.; Huang, H. Discovering forest height changes based on spaceborne lidar data of ICESat–1 in 2005 and ICESat–2 in 2019: A case study in the Beijing–Tianjin–Hebei region of China. *For. Ecosyst.* **2020**, *7*, 53. [CrossRef]

62. Sexton, J.O.; Song, X.P.; Feng, M.; Noojipady, P.; Anand, A.; Huang, C.; Kim, D.H.; Collins, K.M.; Channan, S.; DiMiceli, C. Global, 30–m resolution continuous fields of tree cover: Landsat–based rescaling of MODIS vegetation continuous fields with lidar–based estimates of error. *Int. J. Digit. Earth* **2013**, *6*, 427–448. [CrossRef]
63. Bolton, D.K.; Coops, N.C.; Wulder, M.A. Investigating the agreement between global canopy height maps and airborne Lidar derived height estimates over Canada. *Can. J. Remote Sens.* **2014**, *39*, 139–151. [CrossRef]
64. Zhu, X.X.; Wang, C.; Nie, S.; Pan, F.F.; Xi, X.H.; Hu, Z.Y. Mapping forest height using photon–counting LiDAR data and Landsat 8 OLI data: A case study in Virginia and North Carolina, USA–ScienceDirect. *Ecol. Indic.* **2020**, *114*, 106287. [CrossRef]
65. Dong, X.Y.; Zhang, Z.C.; Yu, R.Y.; Tian, Q.J.; Zhu, X.C. Extraction of Information about Individual Trees from High–Spatial–Resolution UAV–Acquired Images of an Orchard. *Remote Sens.* **2020**, *12*, 133. [CrossRef]
66. Martin, Q.; Joanne, C.W.; Nicholas, C.C. Comparing airborne and spaceborne photon–counting LiDAR canopy structural estimates across different boreal forest types. *Remote Sens. Environ.* **2021**, *262*, 112510.
67. Montesano, P.M.; Rosette, J.; Sun, G.; North, P.; Nelson, R.F.; Dubayah, R.O.; Ranson, K.J.; Kharuk, V. The uncertainty of biomass estimates from modeled ICESat–2 returns across a boreal forest gradient. *Remote Sens. Environ.* **2015**, *158*, 95–109. [CrossRef]
68. Martin, B.; Compton, J.T.; Ankit, K.; Kjeld, R.; Christin, A.; Jennifer, S.; Jerome, C.; Laura, V.R.; Pierre, H.; Abdoul, A.D.; et al. An unexpectedly large count of trees in the West African Sahara and Sahel. *Nature* **2020**, *587*, 78–82.
69. Nie, S.; Wang, C.; Xi, X.H.; Luo, S.Z.; Zhu, X.X.; Li, G.Y.; Liu, H.; Tian, J.Y.; Zhang, S. Assessing the Impacts of Various Factors on Treetop Detection Using LiDAR–Derived Canopy Height Models. *IEEE Trans. Geosci. Remote* **2019**, *57*, 10099–10115. [CrossRef]